

# 44 GHz CLASS I METHANOL (CH<sub>3</sub>OH) MASER SURVEY IN THE GALACTIC CENTER

BRIDGET C. MCEWEN

The Department of Physics and Astronomy, The University of New Mexico, Albuquerque, NM, 87131

LORÁNT O. SJOUWERMAN

National Radio Astronomy Observatory, P.O. Box O, 1003 Lopezville Rd., Socorro, NM, 87801

YLVA M. PIHLSTRÖM

The Department of Physics and Astronomy, The University of New Mexico, Albuquerque, NM, 87131

*Draft version November 5, 2018*

## ABSTRACT

We report on a large 44 GHz ( $7_0 - 6_1$  A<sup>+</sup>) methanol (CH<sub>3</sub>OH) maser survey of the Galactic Center (GC). The Karl G. Jansky Very Large Array was used to search for CH<sub>3</sub>OH maser emission covering a large fraction of the region around Sgr A. In 25 pointings, over 300 CH<sub>3</sub>OH maser sources ( $> 10\sigma$ ) were detected. The majority of the maser sources have a single peak emission spectrum with line of sight velocities that range from about  $-13 \text{ km s}^{-1}$  to  $72 \text{ km s}^{-1}$ . Most maser sources were found to have velocities around  $35\text{--}55 \text{ km s}^{-1}$ , closely following velocities of neighboring interacting molecular clouds. The full width half maximum of each individual spectral feature is very narrow ( $\sim 0.85 \text{ km s}^{-1}$  on average). In the north, where Sgr A East is known to be interacting with the  $50 \text{ km s}^{-1}$  molecular cloud, more than 100 44 GHz CH<sub>3</sub>OH masers were detected. In addition, three other distinct concentrations of masers were found, which appear to be located closer to the interior of the interacting molecular clouds. Possibly a subset of masers are associated with star formation, although conclusive evidence is lacking.

*Subject headings:* masers – ISM: supernova remnants – ISM: individual objects (Sgr A East) – masers – radio lines: ISM

## 1. INTRODUCTION

Astronomical masers form under specific physical conditions and are useful to trace different environments in the interstellar medium (ISM). Interstellar masers are often found in environments such as star forming regions (SFRs) and supernova remnants (SNRs). For example, a detection of a collisionally pumped 1720 MHz hydroxyl (OH) maser has traditionally been used as a tracer of shocked regions produced by the interaction of a SNR with a neighboring molecular cloud (MC) (e.g., Claussen et al. 1997; Frail & Mitchell 1998; Yusef-Zadeh et al. 2003). Another example are the radiatively pumped Class II methanol (CH<sub>3</sub>OH) masers lines, which are typically found near young massive stars. In addition, collisionally pumped Class I CH<sub>3</sub>OH masers are typically found associated with SNRs and outflows in SFRs (e.g., Beuther et al. 2002; Voronkov et al. 2006; Cyganowski et al. 2009; Fontani et al. 2010; Sjouwerman et al. 2010; Pihlström et al. 2014; Sanna et al. 2015). Similar to the 1720 MHz OH masers, the Class I 36 and 44 GHz CH<sub>3</sub>OH maser transitions have also been detected near shocked regions where SNRs are known to be interacting with MCs (e.g., Sjouwerman et al. 2010; Pihlström et al. 2011, 2014).

Recent modeling of Class I CH<sub>3</sub>OH masers in a SNR environment shows that optimal masing conditions for the 44 GHz transition are temperatures  $\geq 50 \text{ K}$  and densities between  $10^4 - 10^6 \text{ cm}^{-3}$ . Similar temperatures but slightly higher densities in the range of  $10^5 - 10^7 \text{ cm}^{-3}$  are the optimal masing conditions for the 36 GHz transi-

tion (McEwen et al. 2014; Nesterenok 2016). Because of the large overlap in conditions, these transitions can be found co-spatially, but brighter 36 GHz CH<sub>3</sub>OH masers are expected to trace higher density regions (e.g., near the actual shock front in SNR/MC interaction regions). This has been supported by observations of bright 36 GHz CH<sub>3</sub>OH masers lining a known shock front in Sgr A East (Sjouwerman et al. 2010; Pihlström et al. 2011).

The Sgr A East SNR is located within the inner 12 pc of our complex Galactic Center (GC) and is known to be interacting with two different giant MCs, M–0.02–0.07 (a.k.a. the  $50 \text{ km s}^{-1}$  cloud) and M–0.13–0.08 (a.k.a. the  $20 \text{ km s}^{-1}$  cloud) (e.g., Mezger et al. 1989; Coil & Ho 2000; Amo-Baladrón et al. 2011). The details of gas transportation in and around the GC are not well understood but different molecular line observations help uncover interaction regions between different environments. For example, the  $50$  and  $20 \text{ km s}^{-1}$  clouds seem to be connected through a ‘Molecular Ridge’, as suggested by an extensive NH<sub>3</sub> study from Coil & Ho (2000), as well as from single dish 36 GHz CH<sub>3</sub>OH observations (Szczeplanski et al. 1991). In addition, observations by McGary et al. (2001) suggest possible connections between the MCs and the Circumnuclear Disk (CND) via streamers. From NH<sub>3</sub> observations by Coil & Ho (2000) it was deduced that, along the line of sight, Sgr A East is pushing this  $50 \text{ km s}^{-1}$  MC eastward and away from us (behind), whereas it also expands into the southern  $20 \text{ km s}^{-1}$  MC at the same time. The southern region of Sgr A East is also interacting with the SNR G359–0.09 (Coil & Ho

2000; Sjouwerman et al. 2008).

These interactions between Sgr A East and its surrounding environment produce collisionally compressed regions of gas some of which are found associated with Class I 36 and 44 GHz  $\text{CH}_3\text{OH}$ , as well as collisionally pumped 1720 MHz OH maser emission (e.g., Yusef-Zadeh et al. 1996; Sjouwerman et al. 2010; Pihlström et al. 2011). It is often speculated that supersonic motions from expanding SNRs may trigger star formation (SF) in neighboring MCs (e.g., Reynoso & Mangum 2001; Cichowolski et al. 2014). Details of the triggering process and what conditions are necessary have never been clearly outlined or confirmed, partly due to the complexity of the regions in the inner Galaxy and the present lack of star forming regions detected in the GC. Different stages of SF can be traced with detections of various maser species, for example, 6.7 GHz, as well as the 44 GHz  $\text{CH}_3\text{OH}$  maser line have been found closely associated with HII regions, outflows, and  $\text{H}_2\text{O}$  masers (typical tracers of SF) (e.g., Kurtz et al. 2004; Moscadelli et al. 2007; Sanna et al. 2010). It is not clear whether Class I  $\text{CH}_3\text{OH}$  masers trace a specific evolutionary stage of SF. Therefore, the detection of maser lines near these regions (such as bright Class I  $\text{CH}_3\text{OH}$  or 22 GHz  $\text{H}_2\text{O}$  lines) may unveil new sites of, and conditions necessary for SF activity in the GC. In addition, the proper understanding of the physical conditions in these regions may also be important for cosmic ray modeling (e.g., Drury et al. 1994; Abdo et al. 2010; Cristofari et al. 2013).

Combining maser observations of SNRs and their surrounding environments along with modeling of conditions necessary for the formation of  $\text{CH}_3\text{OH}$  masers in SNRs, physical conditions of the gas where  $\text{CH}_3\text{OH}$  is detected can be constrained (McEwen et al. 2014). In this context, by studying the distribution of different maser transitions near Sgr A East, we aim to investigate the presence of distinct gas motions in the GC, as well as possibly uncover new sites of star formation. In this study, we report on an extensive 44 GHz  $\text{CH}_3\text{OH}$  maser emission survey of Sgr A East and its surrounding environment taken with the Very Large Array (VLA). A 36 GHz  $\text{CH}_3\text{OH}$  maser survey towards the same region along with a full analysis of the combined 36 and 44 GHz maser detections will be reported on in a future publication.

## 2. 44 GHz VLA OBSERVATIONS AND CALIBRATION

We are reporting on the results from Q-band VLA observations (project code S3115) of the SNR Sgr A East and its surrounding environment. The Q-band B configuration observations were taken on April 20 and 23, 2011 to observe the  $J = 7_0 \rightarrow 6_1 A^+$  rotational transition of  $\text{CH}_3\text{OH}$  at the rest frequency of 44.069 GHz. Figure 1 displays the 25 pointing positions overlaid on a 1720 MHz continuum image of the Sgr A region. The VLA primary beam is  $1.02'$  at 44 GHz, with a typical synthesized beam size of  $0.38'' \times 0.19''$ . The 25 pointings covered a region of roughly  $8' \times 6'$ . Although the area is not Nyquist sampled, regions in between different pointings were also searched for potential masers by imaging beyond the primary beam. These candidate sources have been considered physical if detected in more than one pointing.

The 44 GHz observations were separated into 256 fre-

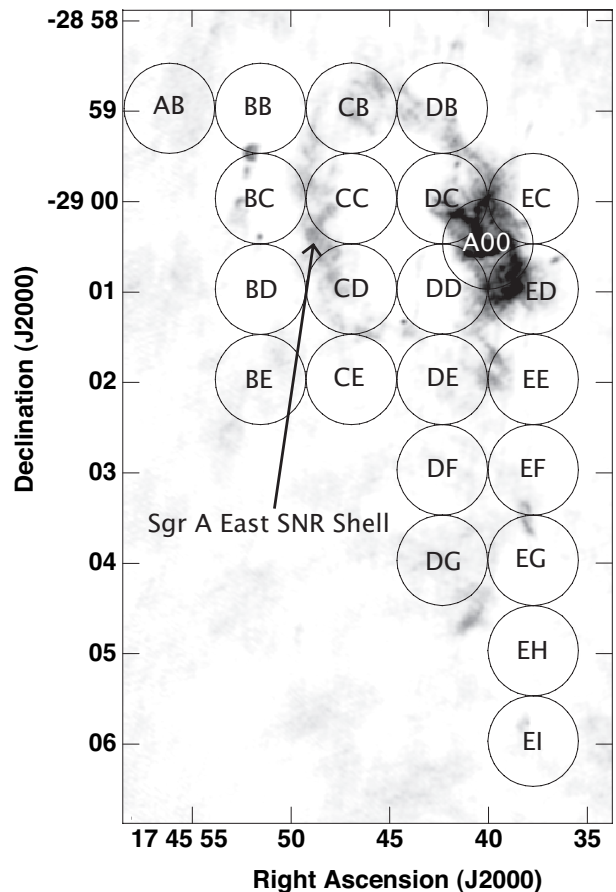


**Figure 1.** 44 GHz VLA observing pointing positions towards the Sgr A region. The ring-like structure pointed at by the arrow outlines the radio continuum emission of the Sgr A East SNR.

quency channels covering 16 MHz of bandwidth. We sampled a velocity range between  $-24$  and  $84 \text{ km s}^{-1}$  with a resolution of about  $0.4 \text{ km s}^{-1}$ . Sgr A\*, located in pointing A00, was used for phase calibration and 3C286 was used as a flux and bandpass calibrator. The total on source time for each pointing including both days of observation was about 8 minutes. Each pointing was individually imaged with  $2048 \times 2048$  pixels of  $0.036''$  for the central 250 channels ( $-23.2$  to  $82.7 \text{ km s}^{-1}$ ). Typical noise rms values were around  $2.9 \text{ mJy beam}^{-1}$  per channel.

The data were reduced, calibrated, and imaged using standard procedures in NRAO's Astronomical Image Processing System (AIPS) pertaining to spectral line data. Fields with bright maser sources ( $> 1 \text{ Jy beam}^{-1}$ ) were self-calibrated in order to improve the dynamic range of the final maps, and to minimize the number of false detections due to side-lobes. The peak flux densities were also corrected for primary beam attenuation using the AIPS task PBCOR.

## 3. RESULTS

### 3.1. Identification Method

Sgr A East is located in a complex and chemically rich environment and many Class I  $\text{CH}_3\text{OH}$  masers have

been previously detected towards various regions near this SNR (Yusef-Zadeh et al. 2008; Sjouwerman et al. 2010; Pihlström et al. 2011; Yusef-Zadeh et al. 2013). In order to search each pointing efficiently, an automated search method using a variety of AIPS tasks was developed to identify maser candidates with flux densities exceeding 10 times the rms noise. These candidates were then sorted according to a confidence in the detection, which depended on the size of the emission region and its signal to noise ratio. The highest ranked candidates were then manually inspected to determine if each was actual emission. Spectral profiles (flux density versus velocity) were produced for the brightest pixel in each region (Fig. 7).

### 3.2. Maser Identification

A total of 318 100% confident 44 GHz CH<sub>3</sub>OH emission regions were found in the 25 pointings. All exceeded a  $10\sigma$  rms noise limit. The spectral parameters of each emission region are presented in Table 1. The coordinates of each source can be found in Columns 3 and 4 (with an estimated positional accuracy of  $\sim 0.5''$ ), which correspond to the peak brightness,  $I_{peak}$  of each emission region (Column 5). Figure 2 shows a histogram of the distribution of the peak flux density values of the maser emission the majority of which are  $\lesssim 0.8$  Jy beam<sup>-1</sup>. The emission was detected across almost the entire region observed with some regions of high concentration. A large abundance of maser emission was detected toward the NE and to the SW, as well as a small amount encompassing the SNR. The maser emission extends to the east about  $2'$  (4.6 pc) from the NE boundary of the SNR shell and about  $5'15''$  (12.1 pc) to the south of the SW boundary of the SNR shell. The majority of emission is unresolved and the brightness temperatures,  $T_b$ , listed in Column 8, are lower limits calculated using the half power beam width of the VLA in B configuration. The minimum brightness temperatures range from  $19 \times 10^2$  to  $52 \times 10^4$  K. The 44 GHz CH<sub>3</sub>OH masers in this study that have previously detected counterparts are indicated in Table 1 with [R].

The peak velocities vary across the region observed, ranging from about  $-13$  to  $72$  km s<sup>-1</sup> and are listed in Column 6. Figure 3 shows two simple histograms of the velocity of maser emission in the NE and SW regions observed separated by a declination of  $-29^\circ 02' 30''$  (between rows E and F in Fig. 1). The color scheme in Fig. 3 represents the different velocities of the emission. The full width half maximum (FWHM) of the brightest peak is listed in Column 7 and was estimated from the number of channels at half  $I_{peak}$  with an error of half of a channel ( $\pm 0.2$  km s<sup>-1</sup>). A gaussian fit was inaccurate to estimate the FWHM because most to the peaks are only a couple channels wide. Instead, we used the number of channels at half peak to approximate an upper limit to the FWHM for each peak. The FWHM of each emission peak listed in Table 1 is narrow ranging from about  $0.4$  to  $3.0$  km s<sup>-1</sup> (1 to 7 channels). These line-widths have similar values to previously detected 44 and 36 GHz CH<sub>3</sub>OH masers in Sgr A East and other SNRs (Sjouwerman et al. 2010; Pihlström et al. 2011). The estimated thermal line-width using the lowest calculated  $T_b$  (1,900 K) is about  $1.6$  km s<sup>-1</sup>. Two sources (119 and 160) have measured

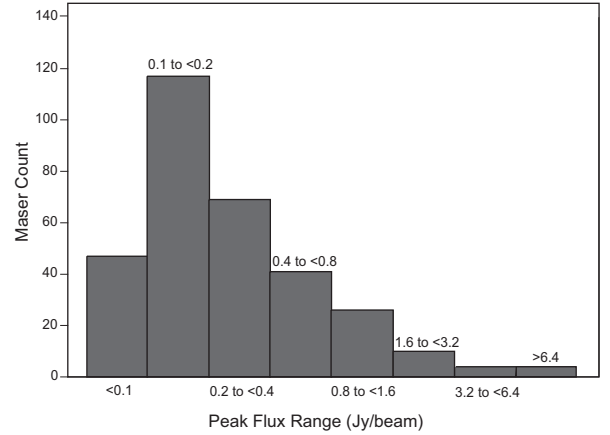


**Figure 2.** A histogram showing the peak flux density distribution of the maser emission.

FWHMs close to the thermal linewidth. A gaussian was fit to the spectral profiles of these two sources but the errors in the fits were large, therefore we conclude that 119 and 160 are not thermal sources. The measured FWHM of the remaining emission regions are less than the calculated thermal line-width for their minimum  $T_b$ , therefore we conclude that all the peaks listed in Table 1 are maser emission and non-thermal in nature.

Although the majority of masers detected were found to be single peaks of emission, as can be seen in Fig. 7, some of the spectra show multiple spectral peaks at a single position ( $\sim 27\%$ ). The sources in Table 1 that are noted with a [M] indicate the sources that display multiple spectral features detected at the same position, some with complicated and broad structure in their spectral profiles. Some of the multiple peak features may imply that we are observing partly unresolved structures within the VLA beam. The emission regions with multiple peaks cover the entire region observed but are mostly concentrated in pointings BB and BC to the NE and EI and EG to the SW. Given the sensitivity of the VLA and the beam size in B-configuration, our observations may not be sensitive to thermal or extended sources below  $4\sigma$  corresponding to a brightness temperature less than  $\sim 370$  K.

## 4. DISCUSSION

Various regions in the Sgr A East environment have previously been searched for different maser transitions. Four collisionally pumped maser transitions have been found, namely the 22 GHz H<sub>2</sub>O, 1720 MHz OH, 36 GHz CH<sub>3</sub>OH, and 44 GHz CH<sub>3</sub>OH lines (Yusef-Zadeh et al. 1996; Sjouwerman et al. 2002; Yusef-Zadeh et al. 2008; Sjouwerman et al. 2010; Pihlström et al. 2011; Yusef-Zadeh et al. 2013). The distribution trends of all these maser species in a few regions will be briefly discussed.

### 4.1. CH<sub>3</sub>OH Maser Distribution

Figure 4 shows the positions of the 44 GHz CH<sub>3</sub>OH maser sources (crosses) detected from this survey within the observed region indicated by the black dashed line, overlaid on a 1720 MHz continuum image. Previously detected 36 GHz (circles) and 44 GHz (triangles) CH<sub>3</sub>OH, 1720 MHz OH (squares), and 22 GHz H<sub>2</sub>O (plus signs)

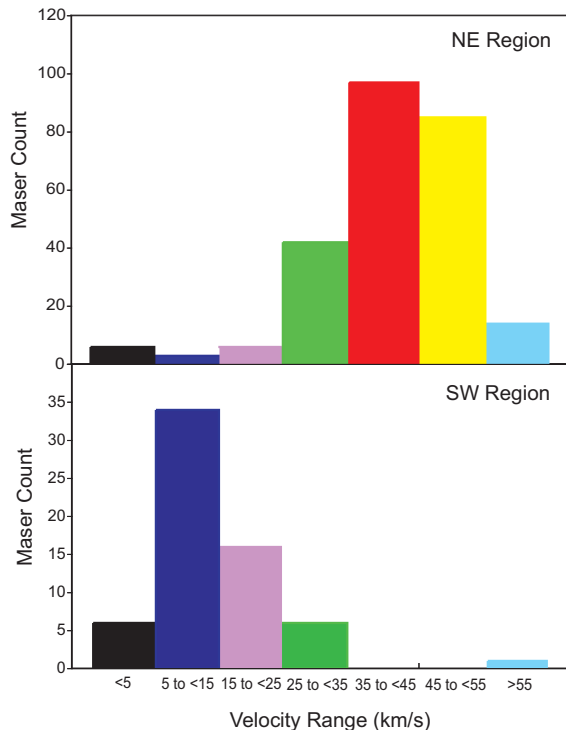


**Figure 3.** Two histograms showing the velocity distribution of the maser emission in the NE (top) and SW (bottom) regions observed. The masers corresponding to these regions are separated by a declination of  $-29^{\circ} 02' 30''$ . The different colors correspond to the velocity of the masers. This color scheme is used in later figures to indicate the velocity of each maser along with their position.

masers are also plotted (Yusef-Zadeh & Mehringer 1995; Yusef-Zadeh et al. 1996; Sjouwerman et al. 2002; Yusef-Zadeh et al. 2008; Sjouwerman et al. 2010; Pihlström et al. 2011; Yusef-Zadeh et al. 2013). The color of each symbol represents the velocity bin of the maser according to the scheme in Fig. 3, for example, light blue symbols represent velocities  $> 55 \text{ km s}^{-1}$ . Typical beam sizes and channel rms values from the previous observations are as follows:  $15''$  and  $15 \text{ mJy beam}^{-1}$  (Yusef-Zadeh et al. 1996),  $2.5'' \times 1.9''$  and  $15 \text{ mJy beam}^{-1}$  (Sjouwerman et al. 2002),  $5.8'' \times 3.9''$  and  $14.1 \text{ mJy beam}^{-1}$  (Pihlström et al. 2008),  $0.2 - 0.4''$  and  $10-12 \text{ mJy beam}^{-1}$  (Sjouwerman et al. 2010),  $1.3'' \times 0.5''$  and  $15-20 \text{ mJy beam}^{-1}$  (Pihlström et al. 2011), and  $1.8'' \times 0.7''$  and  $2.5 \text{ mJy beam}^{-1}$  (Yusef-Zadeh et al. 2013). The previously detected 44 GHz  $\text{CH}_3\text{OH}$  masers from Pihlström et al. (2011) and Yusef-Zadeh et al. (2008) were also detected in this survey and consistent within our positional accuracy, and have velocities within  $\pm 2 \text{ km s}^{-1}$  of our listed  $V_{\text{peak}}$ . Figure 4 shows that the majority of emission has velocities around  $10 \text{ km s}^{-1}$  to the SW region and around  $45 \text{ km s}^{-1}$  to the NE region of the Sgr A East shell.

The most noteworthy result from this survey is the large number of  $\text{CH}_3\text{OH}$  masers detected within the inner parsecs of our GC. The  $\text{CH}_3\text{OH}$  maser emission detected in other Galactic SNRs interacting with MCs pales in comparison to Sgr A East. For example, in a targeted search towards the SNR W28, few 36 and 44 GHz  $\text{CH}_3\text{OH}$  masers were found. Towards the SNR G1.4-0.1, which is interacting with at least 2 MCs, only 36 GHz

$\text{CH}_3\text{OH}$  maser emission was detected, and none at 44 GHz (Pihlström et al. 2014). It is widely accepted that  $\text{CH}_3\text{OH}$  forms on the surface of icy dust grains and then is released into the gas-phase via some heating mechanism, for example, through UV radiation, shocks from cloud-cloud interactions, SNR-cloud interactions, by expanding HII regions, and by young and old stellar outflows (e.g., Garrod 2008; Whittet et al. 2011; Gómez-Ruiz et al. 2016; Yusef-Zadeh et al. 2013). This enhancement of  $\text{CH}_3\text{OH}$  detected near Sgr A East may not be surprising because the GC is extremely chemically rich and subject to shocks. In addition, the enhancement of  $\text{CH}_3\text{OH}$  may be driven by cosmic ray irradiation, more so than in other regions of the Galaxy where the cosmic ray ionization rate is lower (Yusef-Zadeh et al. 2013; Pihlström et al. 2014; Mills et al. 2015).

#### 4.1.1. NE Region

A high concentration of masers is found in the NE region of Sgr A East, where this SNR is interacting with the  $50 \text{ km s}^{-1}$  MC and borders the radio continuum shell of Sgr A East, as can be seen in Fig. 5 (zoom of the red, boxed region in Fig. 4). The vast majority of the 44 GHz masers in this clump are found to have velocities similar to that of the MC, around  $50 \text{ km s}^{-1}$  or less (red and yellow symbols). Many of these masers are coincident with a known shock front (Pihlström et al. 2011) and they seem to follow a sharp boundary along the edge of the SNR radio continuum emission, outlined by the black rectangle in Fig. 5. The brightest 44 GHz  $\text{CH}_3\text{OH}$  masers detected in this region, with  $I_{\text{peak}}$  between  $5.87$  and  $16.16 \text{ Jy beam}^{-1}$ , are significantly weaker than the brightest 36 GHz  $\text{CH}_3\text{OH}$  masers detected in the same region. The lowest flux density ratios between these two maser species in this region is  $\sim 5$ . Based on modeling results from McEwen et al. (2014), this implies a high density region ( $n > 10^6 \text{ cm}^{-3}$ ). In addition, the high concentration of masers in this region is spatially coincident with strong SiO ( $2 - 1$ ) emission (between  $20$  and  $50 \text{ km s}^{-1}$ ), as can be seen in Yusef-Zadeh et al. (2013), which is also indicative of high density shocked gas. Very few masers are detected to the west (right) of this boundary, which is in agreement with what was seen by Pihlström et al. (2011). This means that the physical conditions to the west of the shock front are not conducive for  $\text{CH}_3\text{OH}$  maser emission. It is possible that there may be a lower abundance of  $\text{CH}_3\text{OH}$  in this region, due to UV photodissociation of the  $\text{CH}_3\text{OH}$  molecule as was speculated by Yusef-Zadeh et al. (2013).

The collisionally excited 1720 MHz OH masers form under similar physical conditions compared to Class I  $\text{CH}_3\text{OH}$ , but are found offset from the  $\text{CH}_3\text{OH}$  maser positions. This means they are most likely formed in different regions in the shocked gas (Pihlström et al. 2008; Pihlström et al. 2014; McEwen et al. 2014). The majority of the 44 GHz masers in the NE region have slightly lower velocity spread compared to the OH masers, which have an average of  $\sim 57 \text{ km s}^{-1}$ , and are located just to the SW of the group of 44 GHz  $\text{CH}_3\text{OH}$  masers (in the rectangle region). This implies that the OH masers are located in a region of the shock that is more turbulent and disturbed, namely in the post shocked gas. This strengthens the same conclusion that was drawn based on previous



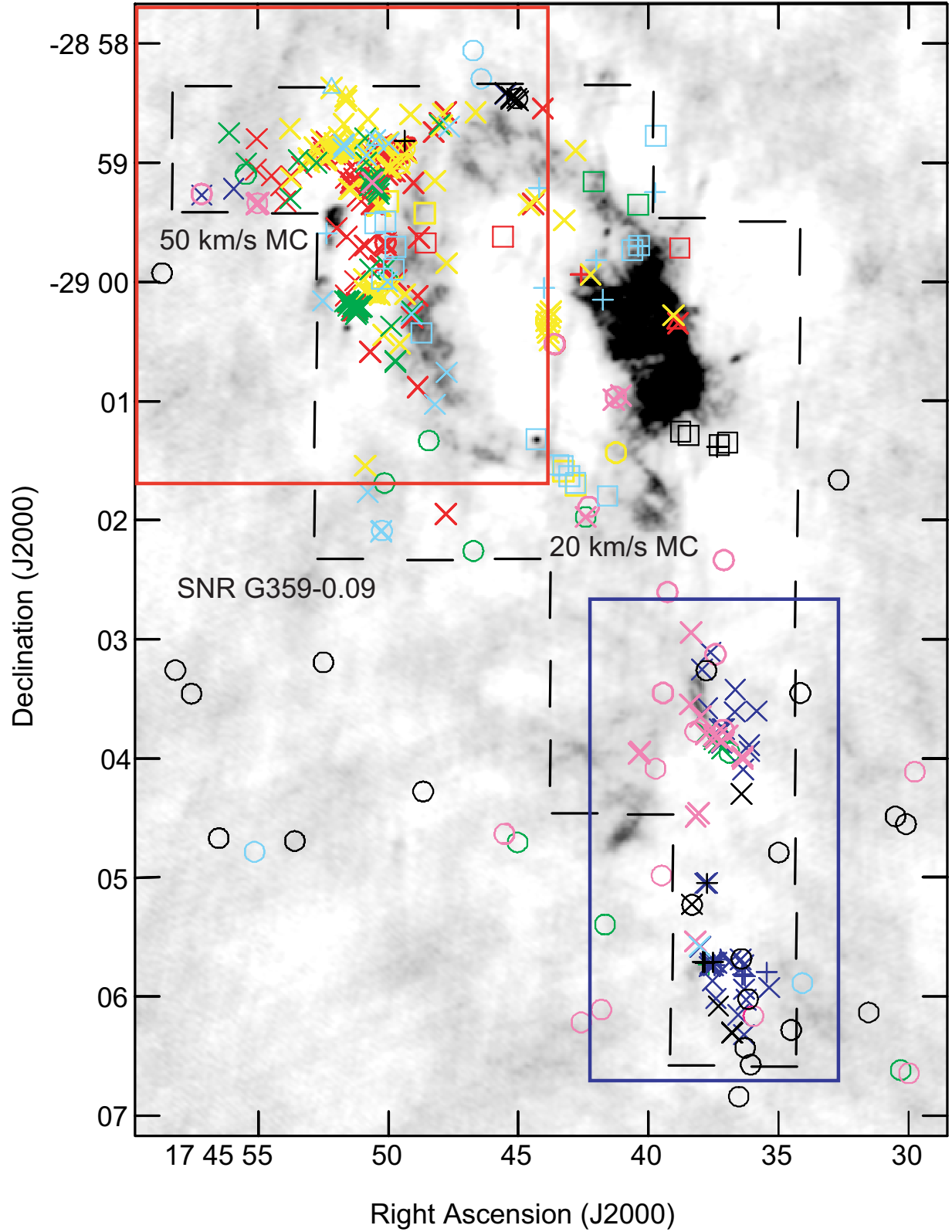


**Figure 4.** Positions of the 44 GHz CH<sub>3</sub>OH masers (crosses) overlaid on a 1720 MHz continuum emission of the Sgr A East environment. In addition, previously detected 44 GHz CH<sub>3</sub>OH (triangles), 36 GHz CH<sub>3</sub>OH (circles), 22 GHz H<sub>2</sub>O (plus-signs), and 1720 MHz OH (squares), masers are overlaid, for details see Yusef-Zadeh & Mehninger (1995); Yusef-Zadeh et al. (1996); Sjouwerman et al. (2002); Yusef-Zadeh et al. (2008); Sjouwerman et al. (2010); Pihlström et al. (2011); Yusef-Zadeh et al. (2013). The color of each symbol represents the velocity of each maser according to the scheme in Fig. 3. The dashed black line indicates the the observed region in this study. The red and blue boxed regions correspond to the enlarged NE and SW regions in Fig. 5 and 6, respectively.

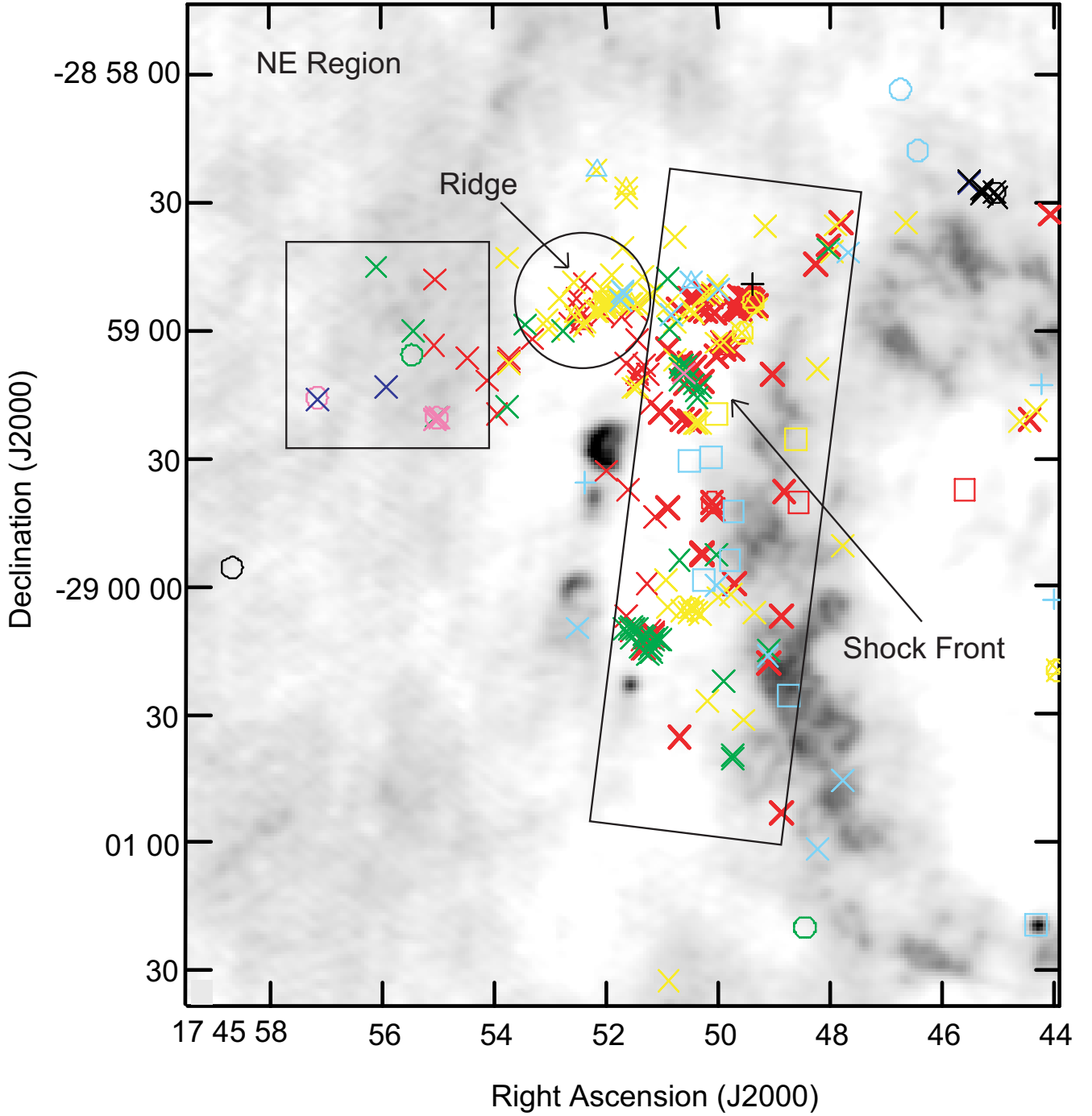


**Figure 5.** Positions of the 44 GHz  $\text{CH}_3\text{OH}$  masers (crosses) overlaid on a 1720 MHz continuum emission of the zoomed in NE region of the Sgr A East environment indicated by the red box in Fig. 4. In addition, previously detected 44 GHz  $\text{CH}_3\text{OH}$  (triangles), 36 GHz  $\text{CH}_3\text{OH}$  (circles), 22 GHz  $\text{H}_2\text{O}$  (plus-signs), and 1720 MHz OH (squares), masers are overlaid, for details see Yusef-Zadeh & Mehringer (1995); Yusef-Zadeh et al. (1996); Sjouwerman et al. (2002); Yusef-Zadeh et al. (2008); Sjouwerman et al. (2010); Pihlström et al. (2011); Yusef-Zadeh et al. (2013). The color of each symbol represents the velocity of each maser according to the scheme in Fig. 3. The black rectangle indicates a large abundance of masers in a region where the  $50 \text{ km s}^{-1}$  MC borders the radio continuum shell. The black circle outlines a cluster of 44 GHz  $\text{CH}_3\text{OH}$  maser emission forming a dense ridge.

but more sparse observations of a CH<sub>3</sub>OH maser survey by Pihlström et al. (2011) and reinforces the idea that bright 36 GHz CH<sub>3</sub>OH masers coincident with weaker 44 GHz CH<sub>3</sub>OH masers detected in a SNR/MC interaction region trace a region closer to the actual shock front compared to OH maser emission.

Just to the east of this front, there appears to be another cluster of 44 GHz CH<sub>3</sub>OH maser emission forming a dense ridge, outlined by the black circle in Fig. 5. Given the distance to the GC of 8.5 kpc, this ridge is about 1.2 pc to the east of the shock front. As suggested by McEwen et al. (2014), these masers may be associated with a possible newly detected young SNR embedded in the 50 km s<sup>-1</sup> MC. In this region, Tsuboi et al. (2011, 2012) detected a dense shocked molecular shell region based on CS (J = 1 – 0) observations and high SiO/H<sup>13</sup>CO<sup>+</sup> ratios. The SiO emission ranges from about 15 to 45 km s<sup>-1</sup>, which agrees with the velocity of the masers. Alternatively, they could be excited by an internal shock in the core of the cloud generated by star formation (SF).

#### 4.1.2. SW Region

Two distinct concentrations of masers are found to the SW of Sgr A East, where this SNR is interacting with the 20 km s<sup>-1</sup> MC (Fig. 6). Here, the vast majority of the 44 GHz masers have velocities that range from 5 to 15 km s<sup>-1</sup> (blue symbols). However, in the northern cluster (outlined by the black square in Fig. 6) several masers are found to have velocities similar to that of the MC, closer to 20 km s<sup>-1</sup> (pink and green symbols) and outline a known non-thermal filament in this region (SgrA-F) (Ho et al. 1985). In the southern cluster (outlined by the black circle) several masers have velocities less than 5 km s<sup>-1</sup> (black symbols), indicating a different origin. The masers in the southern cluster form a rough circle centered around a declination of  $-29^{\circ} 05' 55''$  and is located about 10'' to the SW of a known HII region (SgrA-G, 17h 45m 38.21s  $-29^{\circ} 05' 45.5''$ ) (Ho et al. 1985). These two distinct clusters can also be seen in SiO (2-1) with comparable velocities around 20 km s<sup>-1</sup> (northern) and 0 km s<sup>-1</sup> (southern), in good agreement with the velocities of other masers in these regions (Tsuboi et al. 2011). The majority of the 36 GHz masers previously detected are around 17 km s<sup>-1</sup> (northern cluster) and around 0 km s<sup>-1</sup> (southern cluster). Given the distance of 8.5 kpc to the GC, the separation between these two clumps is about 5.8 pc. The scale of both of these clusters is roughly the same,  $\sim 1.6$  pc, which is about double the size of a typical compact HII region (Kurtz 2005). No 1720 MHz OH masers are detected near these two clusters.

#### 4.2. Possible Star Formation Near Sgr A East

Observationally, 44 GHz CH<sub>3</sub>OH lines are found to be more common and brighter near SF regions compared to the 36 GHz line, although both transitions have been found co-located (e.g., Voronkov et al. 2014). It is not clear whether the Class I CH<sub>3</sub>OH maser traces a specific evolutionary stage of SF. Voronkov et al. (2014) suggest that Class I CH<sub>3</sub>OH masers may be found at multiple epochs throughout the evolution of a massive star. They find Class I CH<sub>3</sub>OH masers near regions with other maser sources that trace early evolutionary stages (e.g.,

6.67 GHz CH<sub>3</sub>OH), as well as older stages (e.g., OH). Another possibility may be that Class I CH<sub>3</sub>OH masers arise from/in different types of shocks in SF regions, including young and old outflows, cloud/cloud collisions, and expanding HII regions (Gómez-Ruiz et al. 2016).

McEwen et al. (2014) show that in a SNR environment (low dust temperature and IR radiation), given a specific CH<sub>3</sub>OH abundance, the 36 GHz maser line dominates at higher number densities and the 44 GHz line at lower densities. These transitions are both collisionally pumped lines, but at lower densities where the 44 GHz line dominates, it is possible that IR pumping may play an important role. If so, it could help explain why the Class I 44 GHz line is more common in SF regions, where IR radiation and dust emission are more prevalent. In fact, modeling by Nesterenok (2016) shows that strong radiation fields can quench other collisionally pumped Class I CH<sub>3</sub>OH lines (e.g., the 25 GHz line), while the radiatively pumped Class II lines (e.g., the 6.7 GHz line) become brighter. However, it is also found that both Class I and Class II masers can be bright and exist in the same region with high IR radiation fields. The modeling work carried out by Nesterenok (2016) did not extend to the 36 and 44 GHz lines. Using the online radiative transfer modeling program (RADEX, van der Tak et al. 2007), taking into account a strong external radiation field (100K) appropriate for SF regions, we indeed find conditions where the 44 GHz and 36 GHz lines simultaneously exist. We also find conditions where the 44 GHz line dominates over the 36 GHz line (e.g., high temperatures  $\sim 200$  K and densities  $\sim 10^4$  cm<sup>-3</sup>). This supports the idea that strong IR radiation fields could influence the production of Class I CH<sub>3</sub>OH lines.

Based on our VLA observations, three regions that are offset from the radio SNR shell can be identified, which will be discussed for possible star formation association. One region is to the NE of the SNR, seemingly located towards interior of the 50 km s<sup>-1</sup> MC, Fig. 5. The other two are to the SW of the SNR near the southern cluster of masers labeled in Fig. 6.

**Region one:** Towards the far NE region outlined by the black square in Fig. 5, there are three recently detected 36 GHz CH<sub>3</sub>OH masers (Yusef-Zadeh et al. 2013). These masers are located more towards the interior of the 50 km s<sup>-1</sup> MC. Two of the masers are spatially coincident with a few 44 GHz masers with similar velocities. In addition, these masers have slightly lower velocities compared to those towards the edge of the Sgr A East shell to the west. Despite searches, radio continuum and H<sub>2</sub>O masers have not been detected in this NE region, which are often signposts of HII regions.

**Region two:** In the SW region (Fig. 6) towards the core of the 20 km s<sup>-1</sup> MC interaction, there is a known HII region (SgrA-G) just to the NW of the the southern cluster where H<sub>2</sub>O masers are detected (Sjouwerman et al. 2002) that have similar velocities to the CH<sub>3</sub>OH masers. The fact that there are both H<sub>2</sub>O masers and 44 GHz CH<sub>3</sub>OH masers in this region suggest possible star formation. It is probable that some of the CH<sub>3</sub>OH masers closer to the HII region are tracing outflows or shocks produced from the expanding HII region.

**Region three:** In the SW southern cluster (Fig. 6), the circular distribution nature of the CH<sub>3</sub>OH masers

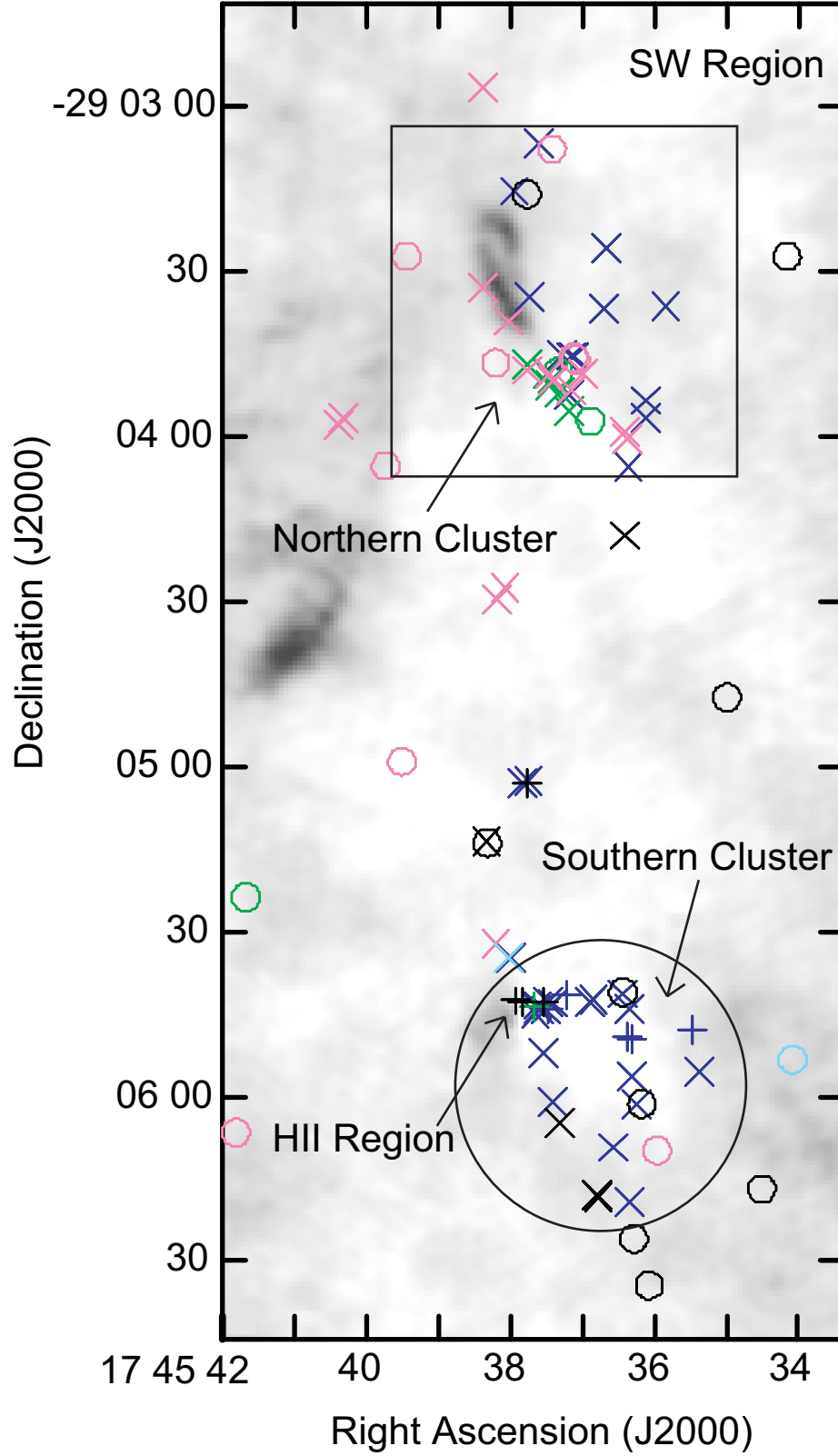


**Figure 6.** Positions of the 44 GHz CH<sub>3</sub>OH masers (crosses) overlaid on a 1720 MHz continuum emission of the zoomed in SW region near Sgr A East indicated by the blue box in Fig. 4. In addition, previously detected 44 GHz CH<sub>3</sub>OH (triangles), 36 GHz CH<sub>3</sub>OH (circles), 22 GHz H<sub>2</sub>O (plus-signs), and 1720 MHz OH (squares), masers are overlaid, for details see Yusef-Zadeh & Mehninger (1995); Yusef-Zadeh et al. (1996); Sjouwerman et al. (2002); Yusef-Zadeh et al. (2008); Sjouwerman et al. (2010); Pihlström et al. (2011); Yusef-Zadeh et al. (2013).



could mean that they are tracing outflows from an undetected SF region (Fig. 6). In addition, no 1720 MHz OH maser emission has been detected in this region, which would be consistent with an early stage of SF. Additional observations of other SF tracers, will hopefully shed light on the properties of this region.

Note that the four known compact HII regions (A-D; Ho et al. 1985) located just to the east of the region outlined by the black rectangle in Fig. 5 are located in the foreground and therefore are not related to the shock front of Sgr A East (Sjouwerman et al. 2008). Although spatially coincident, the few 44 GHz CH<sub>3</sub>OH masers and one H<sub>2</sub>O maser are not associated with these HII regions.

## 5. CONCLUSIONS

Over 300 masers were detected in the Sgr A East region at 44 GHz. The majority of the maser emission is found to be associated with the interaction of the SNR with the neighboring MCs to the NE and SW of the SNR. We summarize the results of this survey in three main points: first, the distribution and abundance of 44 GHz CH<sub>3</sub>OH masers is very different compared to the 1720 MHz OH masers. The 44 GHz CH<sub>3</sub>OH masers are much more abundant than OH and are not found co-spatial with the 1720 MHz OH masers, which suggests they are sustained in different regions of the shocked environment. Second, the brightest 44 GHz CH<sub>3</sub>OH masers detected in this study are significantly weaker compared to the brightest 36 GHz CH<sub>3</sub>OH masers detected in the same region, located in the NE shocked region of Sgr A East, which indicates a high density. Third, it is possible that some of the masers are tracing sites of star formation, although conclusive evidence does not exist at this time. A more complete survey of 36 GHz maser emission is underway, and will be used to complete a full analysis of this region.

We thank NASA for support under FERMI grant NNX12AO77G. B.C.M. acknowledges support from the NM Space Grant Consortium under the Graduate Research Fellowship program. The National Radio Astronomy Observatory is a facility of the National Science Foundation operated under cooperative agreement by Associated Universities, Inc.

## REFERENCES

- Abdo, A.A., Ackermann, M., Ajello, M., et al. 2010, *ApJ*, 718, 348
- Amo-Baladrón, M. A., Martín-Pintado, J., & Martín, S. 2011, *A&A*, 526, A54
- Beuther, H., Walsh, A., Schilke, P., et al. 2002, *A&A*, 390, 289
- Cichowolski, S., Pineault, S., Gamen, R., et al. 2014, *MNRAS*, 438, 1089
- Claussen, M.J., Frail, D.A., Goss, W.M., & Gaume, R.A. 1997, *ApJ*, 489, 143
- Cristofari, P., Gabici, S., Casanova, S., Terrier, R., & Parizot, E., 2013, *MNRAS*, 434, 2748
- Coil, A. L., & Ho, P. T. P. 2000, *ApJ*, 533, 245
- Cyganowski, C. J., Brogan, C. L., Hunter, T. R., & Churchwell, E. 2009, *ApJ*, 702, 1615
- Drury, L. O’C., Aharonian, F.A., & Voelk, H.J., 1994, *A&A*, 287, 959
- Fontani, F., Cesaroni, R., & Furuya, R. S. 2010, *A&A*, 517, A56
- Frail, D.A., & Mitchell, G.F., 1998, *ApJ*, 508, 690
- Garrod, R. T. 2008, *A&A*, 491, 239
- Gómez-Ruiz, A. I., Kurtz, S. E., Araya, E. D., Hofner, P., & Loinard, L. 2016, *ApJS*, 222, 18
- Ho, P. T. P., Jackson, J. M., Barrett, A. H., & Armstrong, J. T. 1985, *ApJ*, 288, 575
- Kurtz, S., Hofner, P., & Álvarez, C. V. 2004, *ApJS*, 155, 149
- Kurtz, S. 2005, *Massive Star Birth: A Crossroads of Astrophysics*, 227, 111
- McEwen, B. C., Pihlström, Y. M., & Sjouwerman, L. O. 2014, *ApJ*, 793, 133
- McGary, R. S., Coil, A. L., & Ho, P. T. P. 2001, *ApJ*, 559, 326
- Mezger, P. G., Zylka, R., Salter, C. J., et al. 1989, *A&A*, 209, 337
- Mills, E. A. C., Butterfield, N., Ludovici, D. A., et al. 2015, *ApJ*, 805, 72
- Moscadelli, L., Goddi, C., Cesaroni, R., Beltrán, M. T., & Furuya, R. S. 2007, *A&A*, 472, 867
- Nesterenok, A. V. 2016, *MNRAS*, 455, 3978
- Pihlström, Y. M., Fish, V. L., Sjouwerman, L. O., et al. 2008, *ApJ*, 676, 371
- Pihlström, Y. M., Sjouwerman, L. O., & Fish, V. L. 2011, *ApJ*, 739, L21
- Pihlström, Y. M., Sjouwerman, L. O., Frail, D. A., et al. 2014, *AJ*, 147, 73
- Reynoso, E. M., & Mangum, J. G. 2001, *AJ*, 121, 347
- Sanna, A., Moscadelli, L., Cesaroni, R., et al. 2010, *A&A*, 517, A78
- Sanna, A., Menten, K. M., Carrasco-González, C., et al. 2015, *ApJ*, 804, L2
- Sjouwerman, L. O., Lindqvist, M., van Langevelde, H. J., & Diamond, P. J. 2002, *A&A*, 391, 967
- Sjouwerman, L. O., & Pihlström, Y. M., 2008, *ApJ*, 681, 1287-1295
- Sjouwerman, L. O., Pihlström, Y. M., & Fish, V. L. 2010, *ApJ*, 710, L111
- Tsuboi, M., Tadaki, K., Miyazaki, A., & Handa, T., 2011, *PASJ*, 63, 763
- Tsuboi, M., & Miyazaki, A., 2012, *PASJ*, 64, 111
- Szczepanski, J. C., Ho, P. T. P., & Gusten, R. 1991, *Atoms, Ions and Molecules: New Results in Spectral Line Astrophysics*, 16, 143
- van der Tak, F. F. S., Black, J. H., Schöier, F. L., Jansen, D. J., & van Dishoeck, E. F. 2007, *A&A*, 468, 627
- Voronkov, M. A., Brooks, K. J., Sobolev, A. M., et al. 2006, *MNRAS*, 373, 411
- Voronkov, M. A., Caswell, J. L., Ellingsen, S. P., Green, J. A., & Breen, S. L. 2014, *MNRAS*, 439, 2584
- Whittet, D. C. B., Cook, A. M., Herbst, E., Chiar, J. E., & Shenoy, S. S. 2011, *ApJ*, 742, 28
- Yusef-Zadeh, F., & Mehringer, D. M. 1995, *ApJ*, 452, L37
- Yusef-Zadeh, F., Roberts, D. A., Goss, W. M., Frail, D. A., & Green, A. J. 1996, *ApJ*, 466, L25
- Yusef-Zadeh, F., Wardle, M., Rho, J., & Sakano, M., 2003, *ApJ*, 585, 319
- Yusef-Zadeh, F., Braatz, J., Wardle, M., & Roberts, D. 2008, *ApJ*, 683, L147
- Yusef-Zadeh, F., Cotton, W., Viti, S., Wardle, M., & Royster, M. 2013, *ApJ*, 764, L19

**Table 1** 44 GHz CH<sub>3</sub>OH Detections

#	Pntg	RA (J2000)	DEC (J2000)	$I_{peak}$ (Jy beam <sup>-1</sup> )	$V_{peak}$ (km s <sup>-1</sup> )	FWHM (km s <sup>-1</sup> )	min $T_b$ (10 <sup>2</sup> K)	Notes
1	EI	17 45 35.36	-29 05 55.5	0.08	+9.2	0.4	26	
2	EG	17 45 35.84	-29 03 36.3	0.12	+6.2	0.8	39	M
3	EG	17 45 36.12	-29 03 56.6	0.07	+11.3	0.4	23	M

## 44 GHz Detections continued ...

#	Pntg	RA (J2000)	DEC (J2000)	$I_{peak}$ (Jy beam $^{-1}$ )	$V_{peak}$ (km s $^{-1}$ )	FWHM (km s $^{-1}$ )	min $T_b$ (10 $^2$ K)	Notes
4	EG	17 45 36.13	-29 03 53.4	0.25	+11.3	0.4	81	
5	EI	17 45 36.24	-29 06 01.6	0.38	+7.5	0.4	120	
6	EI	17 45 36.32	-29 05 56.4	0.06	+6.6	0.4	19	
7	EI	17 45 36.33	-29 06 19.2	0.18	+10.9	0.4	58	
8	EI	17 45 36.34	-29 05 44.2	0.06	+9.6	0.8	19	
9	EG	17 45 36.36	-29 04 05.6	0.08	+6.6	0.4	26	
10	EG	17 45 36.37	-29 04 00.4	0.20	+16.8	0.4	65	
11	EG	17 45 36.40	-29 03 59.2	0.09	+20.6	0.4	29	
12	EG	17 45 36.42	-29 04 18.0	0.09	+1.5	0.4	29	
13	EI	17 45 36.45	-29 05 41.4	0.09	+6.6	0.8	29	
14	EI	17 45 36.56	-29 06 09.3	0.09	+9.2	0.4	29	
15	EG	17 45 36.66	-29 03 25.6	0.10	+6.6	0.4	32	
16	EG	17 45 36.69	-29 03 36.7	0.13	+6.6	0.4	42	
17	EG	17 45 37.11	-29 03 45.4	0.25	+13.8	0.4	81	M
18	EI	17 45 36.78	-29 06 18.4	1.25	-4.4	0.4	400	
19	EI	17 45 36.79	-29 06 18.1	1.22	-5.7	2.8	390	M
20	EI	17 45 36.79	-29 06 18.1	0.68	-4.9	1.6	220	M
21	EI	17 45 36.84	-29 05 42.3	1.17	+13.0	0.8	380	
22	EI	17 45 36.89	-29 05 42.9	0.11	+11.7	0.4	36	
23	EG	17 45 36.98	-29 03 48.6	0.17	+21.9	0.4	55	
24	EG	17 45 37.12	-29 03 45.4	0.44	+14.3	0.4	140	
25	EG	17 45 37.15	-29 03 45.4	0.22	+14.3	1.6	71	M
26	EG	17 45 37.16	-29 03 51.4	0.08	+15.5	0.4	26	
27	EG	17 45 37.17	-29 03 55.2	0.11	+27.9	0.4	36	
28	EG	17 45 37.18	-29 03 52.3	0.09	+14.7	0.4	29	
29	EG	17 45 37.27	-29 03 45.2	0.11	+12.1	0.4	36	
30	EG	17 45 37.30	-29 03 52.1	0.17	+29.6	0.8	55	
31	EI	17 45 37.31	-29 06 04.8	0.07	-2.7	0.8	23	
32	EI	17 45 37.40	-29 05 43.1	0.15	+10.9	0.4	48	
33	EG	17 45 37.40	-29 03 49.8	0.08	+24.9	0.4	26	
34	EI	17 45 37.41	-29 06 01.0	0.16	+7.5	0.4	52	
35	EG	17 45 37.42	-29 03 49.4	0.07	+25.7	0.4	23	
36	EG	17 45 37.46	-29 03 48.4	0.07	+23.6	0.4	23	
37	EG	17 45 37.46	-29 03 50.5	0.54	+25.7	0.4	170	
38	EI	17 45 37.47	-29 05 42.9	0.42	+11.3	0.4	140	
39	EG	17 45 37.49	-29 03 48.7	2.85	+25.3	0.4	920	M
40	EI	17 45 37.50	-29 05 44.3	2.12	+12.1	0.4	680	M
41	EI	17 45 37.54	-29 05 52.2	0.30	+6.2	0.8	97	
42	EI	17 45 37.60	-29 05 44.2	0.17	+12.6	0.4	55	
43	EF	17 45 37.61	-29 03 06.7	0.10	+6.2	0.4	32	
44	EI	17 45 37.62	-29 05 43.5	0.63	+13.8	0.4	200	
45	EI	17 45 37.65	-29 05 45.0	0.20	+14.7	0.4	65	
46	EG	17 45 37.73	-29 03 34.7	0.06	+6.2	0.4	19	M
47	EH	17 45 37.75	-29 05 02.8	0.77	+13.8	0.4	250	
48	EG	17 45 37.76	-29 03 46.8	0.22	+26.6	0.4	71	
49	EG	17 45 37.77	-29 03 47.9	0.25	+24.5	0.4	81	
50	EH	17 45 37.82	-29 05 03.1	0.38	+13.4	0.4	120	
51	EF	17 45 37.94	-29 03 15.3	1.92	+6.6	0.4	620	
52	EI	17 45 38.00	-29 05 34.9	0.13	+14.3	0.4	42	
53	EG	17 45 38.01	-29 03 39.0	0.14	+21.5	0.4	45	
54	EI	17 45 38.03	-29 05 34.8	0.53	+61.0	1.2	170	
55	EH	17 45 38.07	-29 04 27.6	0.39	+24.9	0.4	130	
56	EH	17 45 38.18	-29 04 29.5	0.13	+23.6	0.4	42	
57	EI	17 45 38.20	-29 05 32.2	0.07	+17.7	0.8	23	
58	EH	17 45 38.33	-29 05 13.7	0.19	+3.2	0.4	61	
59	EF	17 45 38.37	-29 02 56.6	0.25	+18.5	0.4	81	
60	EG	17 45 38.39	-29 03 32.9	0.14	+15.5	0.8	45	M
61	AA	17 45 38.86	-29 00 20.9	0.92	+43.6	0.4	300	R
62	AA	17 45 39.03	-29 00 16.9	0.06	+48.7	0.8	19	R
63	DG	17 45 40.31	-29 03 56.7	0.28	+19.8	0.4	90	
64	DG	17 45 40.37	-29 03 57.7	0.30	+16.0	0.4	97	
65	DD	17 45 41.05	-29 00 57.4	0.21	+15.1	0.4	68	
66	DD	17 45 41.32	-29 00 59.3	0.20	+18.1	1.2	65	
67	DC	17 45 42.22	-28 59 56.4	0.07	+48.3	0.4	23	
68	DE	17 45 42.41	-29 01 58.5	0.12	+24.9	0.4	39	
69	DB	17 45 42.80	-28 58 53.9	0.12	+47.9	0.4	39	
70	DB	17 45 43.23	-28 59 29.0	0.08	+49.6	0.4	26	
71	DC	17 45 43.74	-29 00 14.9	0.29	+53.8	0.4	94	R
72	DC	17 45 43.78	-29 00 18.0	0.14	+51.3	0.4	45	
73	DD	17 45 43.80	-29 00 29.5	0.63	+47.0	0.8	200	
74	DC	17 45 43.85	-29 00 25.8	0.12	+49.6	0.4	39	
75	DC	17 45 43.88	-29 00 16.6	0.22	+53.4	0.4	71	
76	DC	17 45 43.90	-29 00 23.0	0.10	+49.1	0.4	32	
77	DC	17 45 43.93	-29 00 19.8	4.80	+49.6	0.4	1600	R
78	DB	17 45 44.05	-28 58 32.8	0.08	+42.3	0.4	26	
79	DB	17 45 44.31	-28 59 18.7	0.09	+49.6	0.4	29	
80	DB	17 45 44.42	-28 59 20.9	0.10	+42.3	0.4	32	

44 GHz Detections continued ...								
#	Pntg	RA (J2000)	DEC (J2000)	$I_{peak}$ (Jy beam <sup>-1</sup> )	$V_{peak}$ (km s <sup>-1</sup> )	FWHM (km s <sup>-1</sup> )	min $T_b$ (10 <sup>2</sup> K)	Notes
81	DB	17 45 44.59	-28 59 21.1	0.11	+49.1	0.4	36	
82	CB	17 45 45.00	-28 58 28.9	0.55	-10.0	0.4	180	M
83	CB	17 45 45.06	-28 58 27.6	1.37	-8.3	2.0	440	M
84	CB	17 45 45.26	-28 58 27.3	1.47	-12.9	0.8	470	
85	CB	17 45 45.27	-28 58 27.9	0.22	-1.9	0.4	71	
86	CB	17 45 45.28	-28 58 26.9	0.23	-7.0	0.4	74	
87	CB	17 45 45.50	-28 58 25.5	0.23	+9.2	0.4	74	M
88	CB	17 45 45.50	-28 58 25.0	0.16	+3.2	0.4	52	
89	CB	17 45 46.63	-28 58 34.7	0.33	+46.2	1.2	110	M
90	CB	17 45 47.66	-28 58 41.7	0.19	+55.9	0.8	61	
91	CC	17 45 47.75	-28 59 50.6	0.07	+53.0	0.4	23	
92	CD	17 45 47.75	-29 00 45.6	0.15	+57.2	0.4	48	
93	CE	17 45 47.78	-29 01 57.1	0.07	+39.8	0.4	23	
94	CB	17 45 47.78	-28 58 34.6	0.58	+39.8	0.8	190	
95	CB	17 45 47.89	-28 58 35.3	0.49	+52.5	1.2	160	M
96	CB	17 45 47.95	-28 58 41.3	0.06	+49.6	0.4	19	
97	CB	17 45 48.01	-28 58 40.0	0.23	+44.0	0.4	74	M
98	CB	17 45 48.02	-28 58 40.8	0.78	+31.3	0.8	250	M
99	CD	17 45 48.21	-29 01 01.7	0.15	+55.9	0.4	48	M
100	CB	17 45 48.21	-28 59 09.1	0.22	+50.4	0.4	71	
101	CB	17 45 48.25	-28 58 44.5	0.37	+43.6	0.4	120	
102	CC	17 45 48.81	-28 59 37.7	0.34	+41.5	0.4	110	
103	CC	17 45 48.86	-29 00 07.1	0.36	+35.5	0.4	120	
104	CD	17 45 48.87	-29 00 53.0	0.12	+41.1	0.4	39	
105	CB	17 45 49.03	-28 59 10.2	0.15	+42.3	0.8	48	
106	BC	17 45 49.08	-29 00 14.9	0.11	+27.4	0.4	36	
107	BC	17 45 49.08	-29 00 18.0	0.12	+36.4	0.4	39	
108	BC	17 45 49.10	-29 00 16.3	0.27	+57.6	0.4	87	
109	BB	17 45 49.14	-28 58 35.7	0.70	+51.7	0.4	230	
110	BB	17 45 49.29	-28 58 54.9	0.68	+48.7	1.2	220	
111	BB	17 45 49.31	-28 58 54.0	0.83	+43.2	0.8	270	
112	BC	17 45 49.35	-29 00 06.3	0.32	+49.6	0.4	100	M
113	BB	17 45 49.36	-28 58 53.3	4.04	+44.9	0.8	1300	R
114	BB	17 45 49.39	-28 58 52.9	2.09	+41.1	0.4	670	M
115	BB	17 45 49.40	-28 58 54.1	0.18	+41.9	0.4	58	M
116	BB	17 45 49.44	-28 58 52.3	1.04	+38.9	2.0	340	M
117	BB	17 45 49.50	-28 58 52.6	0.21	+44.9	1.6	68	M
118	BB	17 45 49.53	-28 58 52.3	0.49	+42.3	0.8	160	
119	BD	17 45 49.54	-29 00 31.3	0.09	+47.9	2.0	29	M
120	BB	17 45 49.56	-28 59 00.6	5.91	+46.2	0.4	1900	M,R
121	BB	17 45 49.60	-28 58 51.9	0.82	+40.6	0.4	260	
122	BB	17 45 49.61	-28 58 55.1	0.18	+42.3	0.4	58	
123	BB	17 45 49.68	-28 58 55.2	16.19	+42.3	0.4	5200	R
124	BC	17 45 49.69	-28 59 59.3	0.14	+37.2	0.4	45	
125	BB	17 45 49.69	-28 58 54.2	0.96	+44.5	0.4	310	
126	BD	17 45 49.73	-29 00 40.4	0.44	+34.7	0.8	140	M
127	BD	17 45 49.73	-29 00 39.7	0.42	+29.6	0.4	140	
128	BB	17 45 49.74	-28 59 04.5	0.22	+44.5	0.4	71	
129	BC	17 45 49.77	-29 00 01.9	1.19	+54.7	0.4	380	M
130	BB	17 45 49.87	-28 59 03.6	0.11	+36.8	0.4	36	
131	BC	17 45 49.88	-29 00 22.3	0.14	+27.4	0.4	45	
132	BB	17 45 49.89	-28 59 04.5	9.95	+36.4	0.4	3200	R
133	BB	17 45 49.90	-28 59 02.6	0.12	+46.6	0.4	39	
134	BB	17 45 49.94	-28 59 02.5	0.12	+41.9	0.8	39	M
135	BB	17 45 49.98	-28 58 50.3	0.69	+58.5	0.4	220	M
136	BC	17 45 49.99	-29 00 02.5	0.10	+47.4	0.4	32	
137	BB	17 45 50.00	-28 58 49.6	0.29	+53.4	0.4	94	
138	BB	17 45 50.02	-28 59 02.8	0.14	+47.0	0.4	45	
139	BC	17 45 50.02	-28 59 52.6	0.25	+34.3	0.4	81	
140	BB	17 45 50.03	-28 59 06.0	1.43	+38.1	0.4	460	
141	BC	17 45 50.03	-28 59 59.9	0.18	+55.1	0.8	58	
142	BB	17 45 50.04	-28 58 55.9	0.15	+42.3	0.4	48	
143	BC	17 45 50.08	-28 59 42.0	0.18	+40.6	0.4	58	
144	BB	17 45 50.08	-28 58 51.0	0.23	+54.7	0.4	74	
145	BB	17 45 50.10	-28 58 51.9	0.18	+43.2	0.4	58	
146	BC	17 45 50.10	-28 59 40.2	0.40	+39.4	0.4	130	
147	BB	17 45 50.15	-28 58 51.4	0.87	+52.1	0.4	280	
148	BD	17 45 50.17	-29 00 26.7	0.09	+49.6	0.4	29	
149	BB	17 45 50.22	-28 58 55.3	0.11	+41.9	0.4	36	
150	BB	17 45 50.25	-28 58 51.6	0.14	+50.8	0.4	45	
151	BE	17 45 50.26	-29 02 05.3	0.70	+67.8	0.8	230	M
152	BB	17 45 50.26	-28 58 51.2	0.58	+42.3	0.8	190	
153	BE	17 45 50.27	-29 02 05.9	0.10	+65.7	0.4	32	
154	BC	17 45 50.28	-28 59 52.1	0.11	+40.2	0.4	36	
155	BB	17 45 50.28	-28 59 11.9	0.14	+41.9	0.4	45	
156	BC	17 45 50.29	-28 59 52.7	0.34	+37.2	0.4	110	
157	BB	17 45 50.30	-28 58 54.9	0.08	+36.4	0.4	26	

## 44 GHz Detections continued ...

#	Pntg	RA (J2000)	DEC (J2000)	$I_{peak}$ (Jy beam $^{-1}$ )	$V_{peak}$ (km s $^{-1}$ )	FWHM (km s $^{-1}$ )	min $T_b$ (10 $^2$ K)	Notes
158	BB	17 45 50.30	-28 59 21.7	0.20	+51.7	0.4	65	
159	BC	17 45 50.32	-29 00 06.4	0.11	+52.1	0.4	36	
160	BB	17 45 50.32	-28 59 13.2	0.10	+31.7	2.4	32	M
161	BB	17 45 50.36	-28 59 15.8	1.13	+34.7	0.4	360	M
162	BC	17 45 50.36	-29 00 05.9	0.36	+47.9	0.4	120	
163	BB	17 45 50.37	-28 59 21.8	0.11	+48.7	0.4	36	
164	BB	17 45 50.38	-28 59 14.0	0.15	+32.6	0.4	48	
165	BB	17 45 50.39	-28 59 08.4	0.43	+42.3	0.4	140	
166	BB	17 45 50.41	-28 59 21.6	1.16	+47.0	0.4	370	M
167	BB	17 45 50.42	-28 58 52.4	0.16	+43.2	0.4	52	M
168	BB	17 45 50.42	-28 59 12.6	0.22	+28.7	0.8	71	
169	BB	17 45 50.44	-28 58 56.1	0.32	+50.0	0.4	100	M
170	BC	17 45 50.45	-29 00 05.5	1.24	+49.1	1.2	400	R
171	BB	17 45 50.47	-28 58 55.0	0.11	+41.9	0.4	36	
172	BB	17 45 50.48	-28 58 48.7	2.70	+58.9	0.8	870	M,R
173	BC	17 45 50.49	-29 00 04.8	2.35	+47.9	2.4	760	
174	BB	17 45 50.49	-28 59 21.2	0.12	+36.4	0.4	39	
175	BB	17 45 50.49	-28 59 07.6	2.45	+41.5	2.0	790	M,R
176	BB	17 45 50.50	-28 58 52.5	0.20	+34.7	0.4	65	
177	BC	17 45 50.52	-29 00 06.0	0.08	+47.9	0.4	26	M
178	BB	17 45 50.52	-28 59 11.5	0.11	+33.0	1.2	36	
179	BB	17 45 50.56	-28 59 08.5	0.79	+33.8	0.4	250	
180	BB	17 45 50.58	-28 59 12.6	0.44	+36.0	0.4	140	
181	BB	17 45 50.59	-28 59 09.0	0.36	+37.2	2.8	120	M
182	BB	17 45 50.60	-28 59 10.0	0.23	+23.2	1.2	74	M
183	BB	17 45 50.62	-28 59 20.8	0.11	+41.9	0.4	36	
184	BB	17 45 50.64	-28 59 07.9	0.13	+27.4	0.4	42	
185	BB	17 45 50.65	-28 59 07.5	0.12	+35.1	0.4	39	M
186	BC	17 45 50.65	-29 00 05.8	0.14	+46.6	0.4	45	
187	BB	17 45 50.66	-28 59 08.8	7.48	+27.0	0.4	2400	M,R
188	BC	17 45 50.68	-28 59 53.9	0.10	+28.3	0.8	32	M
189	BD	17 45 50.68	-29 00 35.4	0.11	+39.4	0.8	36	M
190	BB	17 45 50.68	-28 59 11.4	0.12	+32.6	0.8	39	
191	BB	17 45 50.69	-28 58 55.1	0.21	+41.9	0.4	68	
192	BB	17 45 50.75	-28 58 58.1	0.10	+46.6	0.4	32	
193	BB	17 45 50.75	-28 59 06.7	0.17	+50.0	0.8	55	M
194	BB	17 45 50.77	-28 58 37.9	0.15	+47.0	0.4	48	
195	BE	17 45 50.78	-29 01 45.9	0.76	+71.7	1.2	250	M
196	BB	17 45 50.83	-28 58 56.2	1.12	+55.5	0.4	360	
197	BB	17 45 50.85	-28 58 59.8	0.45	+30.4	0.4	150	M
198	BE	17 45 50.88	-29 01 32.6	0.14	+46.2	0.4	45	
199	BC	17 45 50.88	-28 59 41.7	0.13	+40.6	0.4	42	
200	BB	17 45 50.88	-28 58 47.7	0.12	+27.0	0.4	39	
201	BB	17 45 50.89	-28 58 54.2	0.09	+47.4	0.4	29	
202	BC	17 45 50.89	-29 00 04.9	0.23	+47.9	0.4	74	
203	BB	17 45 50.90	-28 59 04.4	0.09	+36.4	0.4	29	
204	BC	17 45 50.92	-28 59 58.6	0.75	+51.3	2.4	240	M
205	BC	17 45 51.01	-29 00 12.6	0.13	+28.7	1.2	42	
206	BB	17 45 51.02	-28 59 19.3	0.13	+44.5	1.2	42	
207	BC	17 45 51.05	-29 00 12.7	0.09	+33.0	0.4	29	
208	BC	17 45 51.07	-29 00 12.0	0.09	+29.6	1.6	29	M
209	BC	17 45 51.12	-28 59 43.6	0.70	+37.7	1.6	230	
210	BC	17 45 51.14	-29 00 11.1	0.10	+39.4	0.4	32	
211	BC	17 45 51.14	-29 00 12.3	0.07	+35.1	0.8	23	M
212	BC	17 45 51.15	-29 00 11.7	0.54	+37.2	0.8	170	
213	BC	17 45 51.16	-29 00 10.8	0.08	+37.2	0.4	26	
214	BC	17 45 51.16	-29 00 12.4	0.16	+34.7	1.2	52	M
215	BC	17 45 51.17	-29 00 13.8	0.13	+34.7	0.4	42	
216	BB	17 45 51.17	-28 58 52.0	0.12	+47.4	1.2	39	
217	BC	17 45 51.18	-29 00 15.5	0.95	+33.4	0.8	310	M
218	BB	17 45 51.19	-28 59 17.1	0.15	+38.9	0.4	48	
219	BC	17 45 51.20	-29 00 12.2	0.17	+39.8	0.4	55	M
220	BC	17 45 51.20	-29 00 10.5	0.31	+38.1	0.8	100	M
221	BC	17 45 51.21	-29 00 14.7	0.09	+34.3	0.8	29	M
222	BC	17 45 51.21	-29 00 11.9	0.25	+42.8	1.2	81	M
223	BB	17 45 51.22	-28 58 51.6	0.15	+47.0	0.8	48	M
224	BC	17 45 51.24	-29 00 16.1	0.27	+33.8	0.4	87	M
225	BB	17 45 51.24	-28 59 10.1	0.15	+38.1	0.4	48	
226	BC	17 45 51.25	-29 00 13.1	0.51	+36.8	1.6	170	
227	BC	17 45 51.26	-28 59 59.5	0.07	+36.4	0.4	23	
228	BC	17 45 51.27	-29 00 12.0	0.94	+39.4	1.2	300	M
229	BC	17 45 51.30	-29 00 14.7	0.25	+36.4	0.4	81	M
230	BB	17 45 51.32	-28 59 08.0	0.26	+44.9	0.4	84	
231	BC	17 45 51.32	-29 00 11.9	0.97	+34.3	0.8	310	M
232	BC	17 45 51.33	-29 00 11.4	0.54	+29.1	0.4	170	
233	BB	17 45 51.34	-28 58 47.4	0.11	+46.6	0.4	36	
234	BC	17 45 51.36	-29 00 14.5	0.11	+35.1	1.2	36	M



44 GHz Detections continued ...								
#	Pntg	RA (J2000)	DEC (J2000)	$I_{peak}$ (Jy beam <sup>-1</sup> )	$V_{peak}$ (km s <sup>-1</sup> )	FWHM (km s <sup>-1</sup> )	min $T_b$ (10 <sup>2</sup> K)	Notes
235	BC	17 45 51.36	-29 00 12.4	0.18	+40.6	0.4	58	
236	BC	17 45 51.39	-29 00 14.3	0.11	+33.4	0.4	36	
237	BB	17 45 51.40	-28 59 11.7	0.19	+41.9	0.4	61	
238	BB	17 45 51.42	-28 59 10.2	1.19	+43.6	0.4	380	M,R
239	BB	17 45 51.43	-28 59 13.3	0.16	+49.6	1.6	52	M
240	BB	17 45 51.43	-28 59 02.1	0.12	+42.3	0.4	39	
241	BC	17 45 51.44	-29 00 10.0	0.64	+30.9	1.2	210	
242	BB	17 45 51.44	-28 58 53.6	0.09	+46.2	0.4	29	
243	BB	17 45 51.45	-28 59 09.7	0.35	+40.6	0.8	110	
244	BB	17 45 51.47	-28 58 54.9	0.07	+41.9	0.4	23	
245	BB	17 45 51.49	-28 59 13.4	0.25	+48.3	0.8	81	
246	BC	17 45 51.50	-29 00 10.0	0.28	+27.4	0.8	90	
247	BB	17 45 51.53	-28 58 53.9	0.53	+45.3	2.4	170	M
248	BC	17 45 51.53	-29 00 09.3	0.18	+29.1	0.4	58	
249	BC	17 45 51.54	-29 00 10.3	0.07	+37.7	0.8	23	
250	BC	17 45 51.54	-29 00 12.0	0.10	+32.1	0.4	32	
251	BC	17 45 51.56	-29 00 10.1	0.09	+28.7	0.8	29	
252	BB	17 45 51.56	-28 58 53.7	2.03	+46.2	1.6	650	R
253	BC	17 45 51.59	-28 59 37.2	0.33	+38.1	0.4	110	
254	BB	17 45 51.62	-28 58 28.6	0.26	+54.2	0.4	84	
255	BB	17 45 51.62	-28 59 07.8	0.49	+41.9	0.4	160	
256	BB	17 45 51.62	-28 58 26.7	0.74	+53.0	0.8	240	R
257	BC	17 45 51.64	-29 00 06.8	0.14	+40.6	0.4	45	
258	BC	17 45 51.66	-29 00 09.8	0.08	+27.4	0.4	26	
259	BB	17 45 51.68	-28 58 51.2	0.71	+60.2	0.4	230	M
260	BB	17 45 51.70	-28 58 40.6	0.19	+46.6	0.4	61	
261	BB	17 45 51.70	-28 58 50.8	0.99	+56.8	0.4	320	
262	BB	17 45 51.71	-28 58 56.6	0.18	+44.9	0.8	58	M
263	BB	17 45 51.72	-28 58 53.0	1.16	+58.5	0.8	370	M
264	BB	17 45 51.75	-28 58 51.8	0.19	+51.7	0.4	61	
265	BB	17 45 51.76	-28 58 52.9	0.16	+53.8	1.2	52	
266	BB	17 45 51.78	-28 58 52.2	0.61	+49.1	0.8	200	
267	BB	17 45 51.88	-28 58 52.9	11.90	+47.0	0.4	3800	R
268	BB	17 45 51.90	-28 58 47.1	0.12	+46.6	0.4	39	M
269	BB	17 45 51.94	-28 58 53.4	0.94	+49.6	0.8	300	M
270	BB	17 45 51.97	-28 58 54.6	0.11	+51.7	2.0	36	M
271	BC	17 45 51.98	-28 59 32.9	0.24	+41.1	0.4	77	
272	BB	17 45 51.99	-28 58 54.4	0.24	+51.7	0.8	77	M
273	BB	17 45 52.00	-28 58 53.1	0.10	+49.1	0.8	32	M
274	BB	17 45 52.02	-28 58 53.9	0.22	+53.4	0.4	71	
275	BB	17 45 52.03	-28 58 54.7	0.47	+50.8	0.8	150	M
276	BB	17 45 52.03	-28 58 53.5	0.29	+48.3	1.2	94	M
277	BB	17 45 52.04	-28 58 55.8	0.18	+38.9	0.4	58	
278	BB	17 45 52.05	-28 58 50.3	0.45	+46.2	0.4	150	M
279	BB	17 45 52.13	-28 58 55.5	2.64	+45.3	0.8	850	M,R
280	BB	17 45 52.16	-28 58 22.4	1.40	+54.7	1.2	450	R
281	BB	17 45 52.19	-28 58 55.3	0.13	+47.9	0.4	42	
282	BB	17 45 52.36	-28 58 58.1	0.72	+45.3	1.2	230	
283	BB	17 45 52.36	-28 58 49.2	0.13	+41.9	1.6	42	M
284	BB	17 45 52.39	-28 58 58.7	0.33	+45.3	0.8	110	M
285	BB	17 45 52.42	-28 58 56.3	0.10	+44.9	0.4	32	
286	BB	17 45 52.43	-28 58 58.2	3.32	+43.2	0.8	1070	M,R
287	BB	17 45 52.46	-28 58 54.9	0.17	+42.3	0.8	55	M,R
288	BC	17 45 52.51	-29 00 09.7	0.36	+68.7	0.8	116	
289	BB	17 45 52.52	-28 58 52.4	0.36	+37.7	0.4	116	
290	BB	17 45 52.55	-28 58 56.8	2.48	+45.3	0.4	800	R
291	BB	17 45 52.56	-28 58 48.5	0.23	+48.7	0.4	74	M
292	BB	17 45 52.62	-28 58 58.5	0.20	+44.0	0.4	65	
293	BB	17 45 52.75	-28 59 00.1	0.11	+31.3	0.4	36	
294	BB	17 45 52.83	-28 58 52.4	0.16	+46.2	0.4	52	
295	BB	17 45 53.03	-28 58 59.6	0.88	+48.3	0.4	280	
296	BB	17 45 53.06	-28 58 57.7	0.15	+46.6	0.4	48	
297	BB	17 45 53.32	-28 59 02.0	0.17	+43.6	0.4	55	
298	BB	17 45 53.44	-28 58 58.6	0.14	+30.0	0.4	45	
299	AB	17 45 53.72	-28 59 07.8	0.11	+47.0	0.4	36	
300	BB	17 45 53.73	-28 59 06.5	0.38	+42.3	0.8	120	
301	AB	17 45 53.74	-28 59 07.2	0.24	+41.5	0.4	77	M
302	AB	17 45 53.74	-28 59 07.1	0.45	+41.5	0.4	150	
303	BB	17 45 53.75	-28 59 18.0	0.36	+29.1	0.4	116	
304	AB	17 45 53.76	-28 58 42.9	0.10	+46.6	0.4	32	
305	AB	17 45 53.94	-28 59 19.6	0.10	+42.3	0.4	32	
306	AB	17 45 54.12	-28 59 11.7	0.09	+38.9	0.4	29	
307	AB	17 45 54.48	-28 59 06.5	0.11	+43.2	0.4	36	
308	AB	17 45 54.97	-28 59 20.4	0.07	+24.5	0.8	23	
309	AB	17 45 55.01	-28 59 20.5	0.12	+18.9	0.8	39	
310	AB	17 45 55.03	-28 59 20.2	0.15	+31.7	0.4	48	
311	AB	17 45 55.04	-28 59 21.0	0.18	+22.3	0.4	58	

44 GHz Detections continued ...								
#	Pntg	RA (J2000)	DEC (J2000)	$I_{peak}$ (Jy beam $^{-1}$ )	$V_{peak}$ (km s $^{-1}$ )	FWHM (km s $^{-1}$ )	min $T_b$ (10 $^2$ K)	Notes
312	AB	17 45 55.05	−28 58 48.0	0.11	+37.2	0.4	36	
313	AB	17 45 55.06	−28 59 20.8	0.39	+16.4	0.8	130	
314	AB	17 45 55.07	−28 59 03.3	0.07	+42.3	0.4	23	
315	AB	17 45 55.44	−28 59 00.2	0.06	+28.3	0.4	19	
316	AB	17 45 55.93	−28 59 13.1	0.31	+13.4	2.8	100	M
317	AB	17 45 56.10	−28 58 45.0	0.38	+27.9	0.4	120	M
318	AB	17 45 57.15	−28 59 16.2	0.54	+10.0	0.4	170	

Notes. (M): Multiple spectral features detected at the same position (above  $10\sigma$ ). The spectral parameters of the brightest peak are listed in this table. (R): This 44 GHz maser emission was previously detected by Yusef-Zadeh et al. (2008) and/or Pihlström et al. (2011). The brightness temperatures,  $T_b$ , listed in column 8 are lower limits.

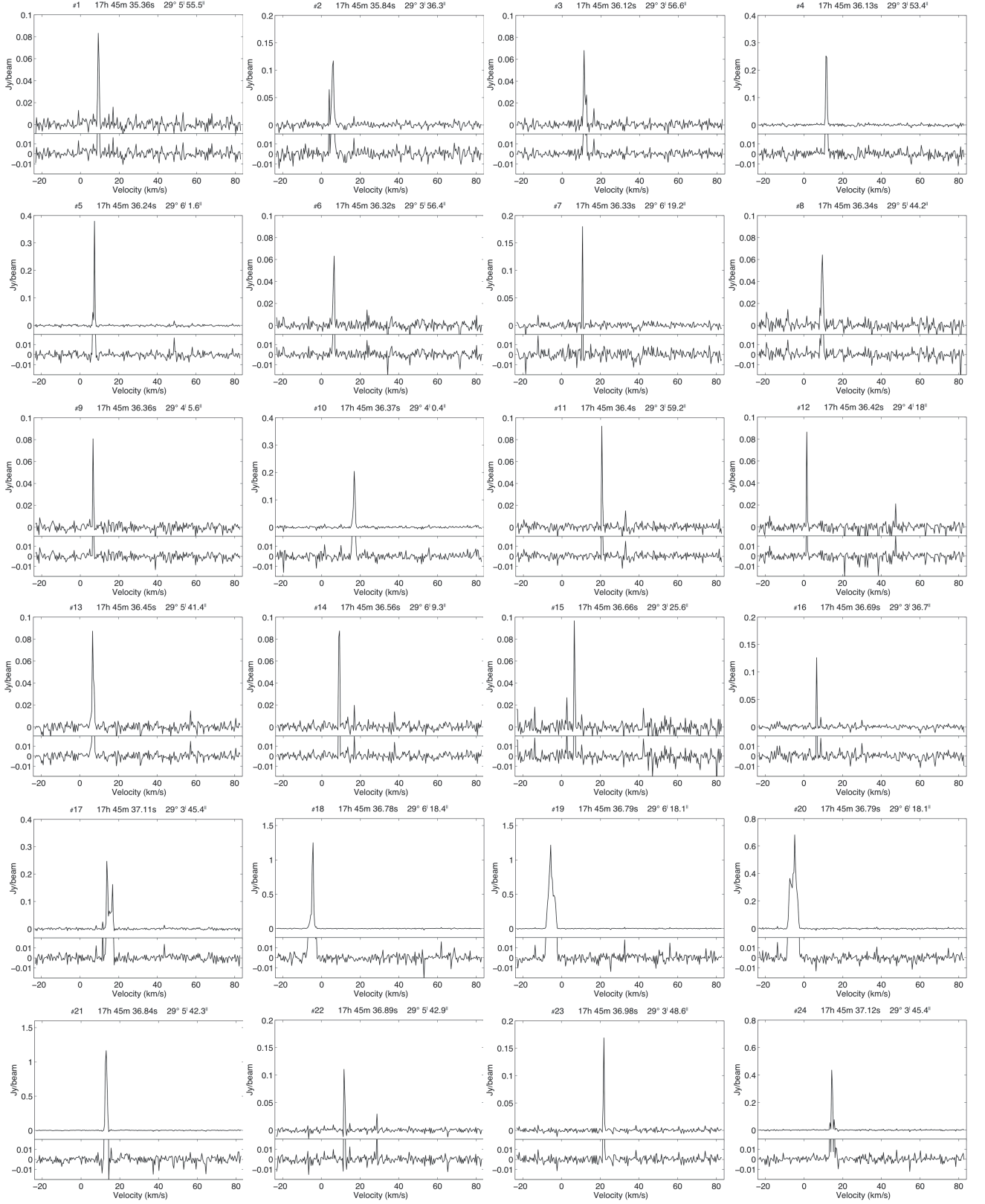


**Figure 7.** Example 44 GHz CH<sub>3</sub>OH maser spectral profiles as a function of LSR line of sight velocity. The bottom row is a fixed scale zoom on the spectral baseline to more predominately show the rms noise and possible multiple spectral lines that may be invisible in the top row auto-scaled spectra. The labels in the header of each spectra are the entry number in Table 1 and the J2000 position of the brightest peak.

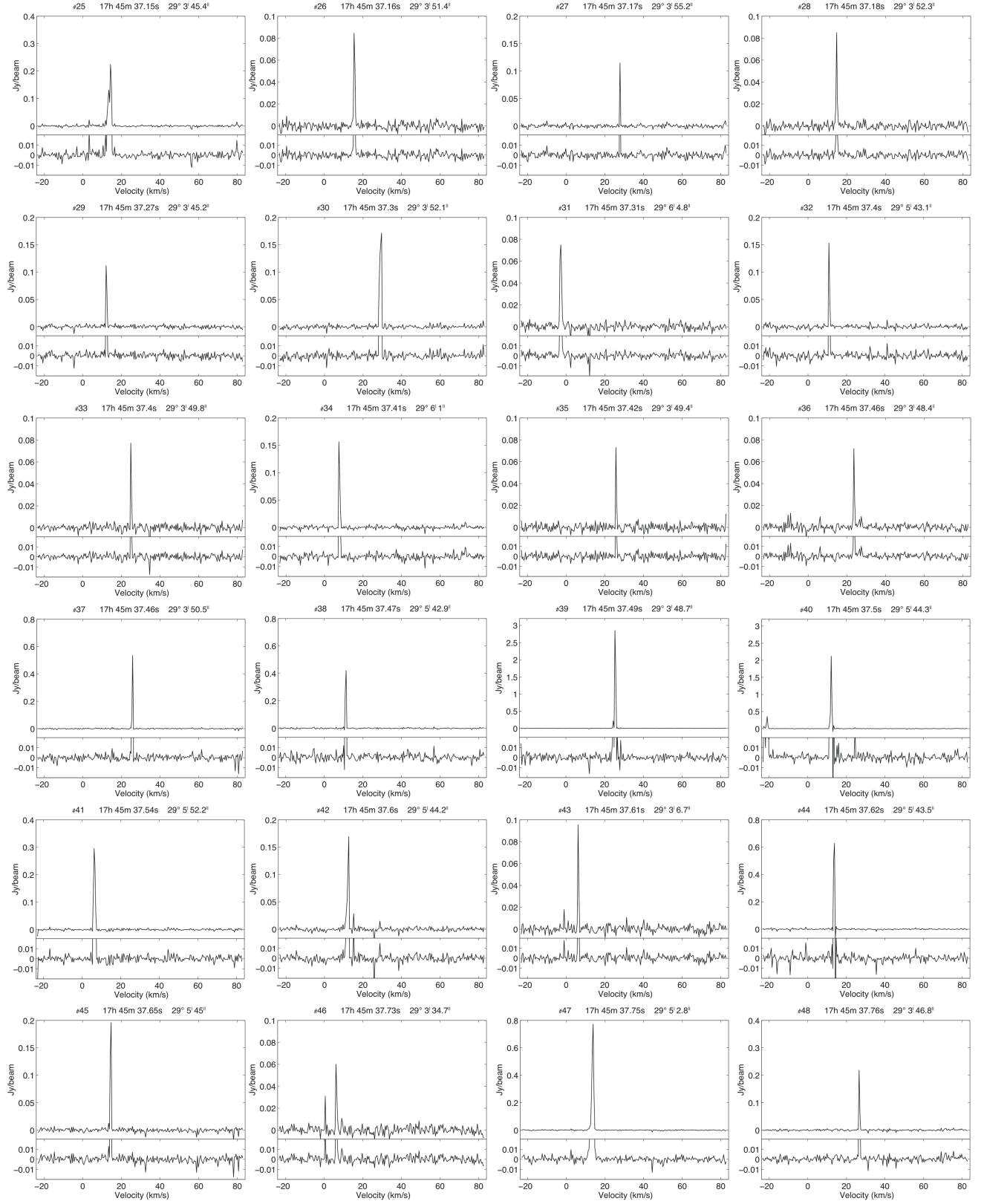
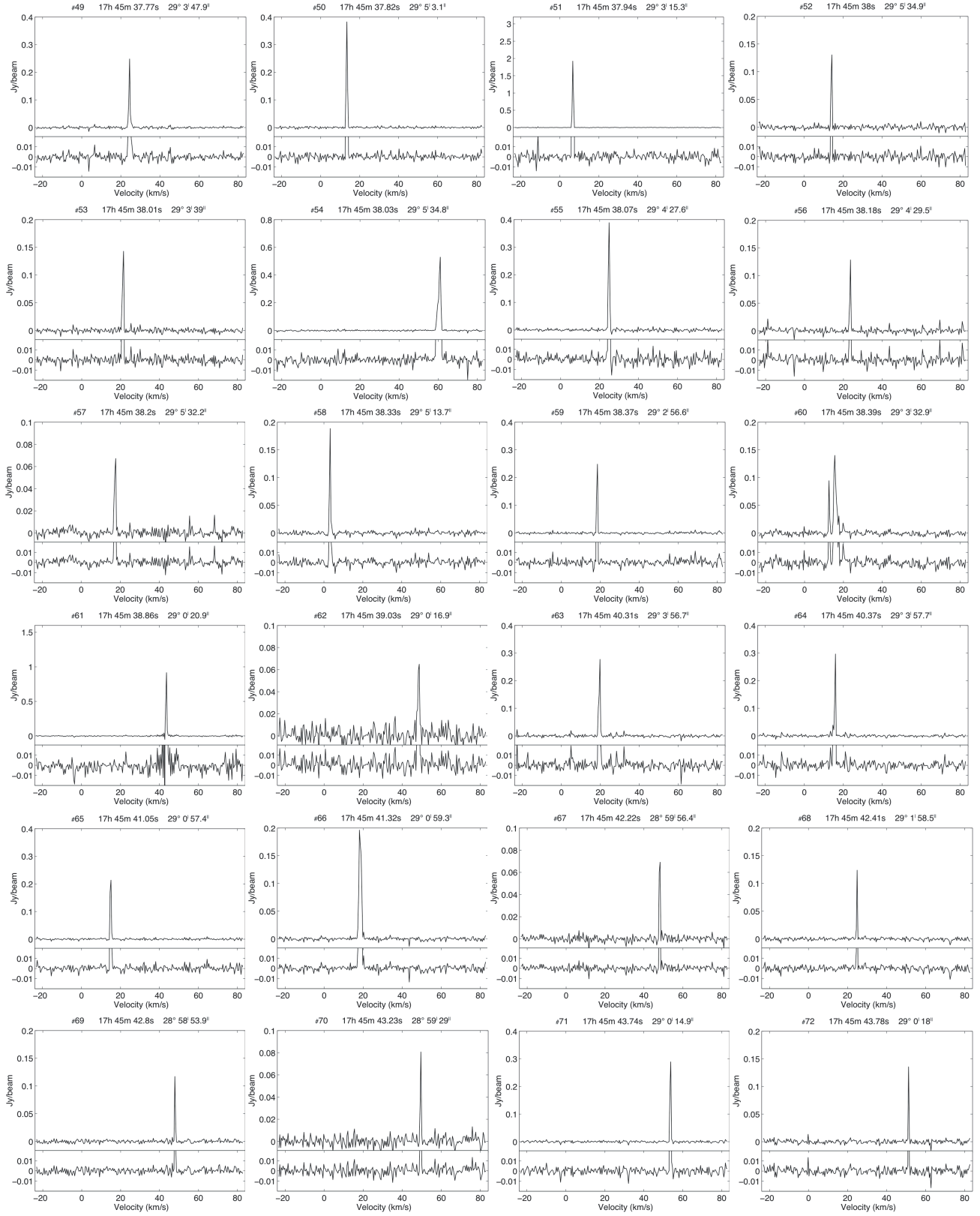


Figure 7. Example 44 GHz  $\text{CH}_3\text{OH}$  maser spectral profiles continued...



Figure 7. Example 44 GHz CH<sub>3</sub>OH maser spectral profiles continued...

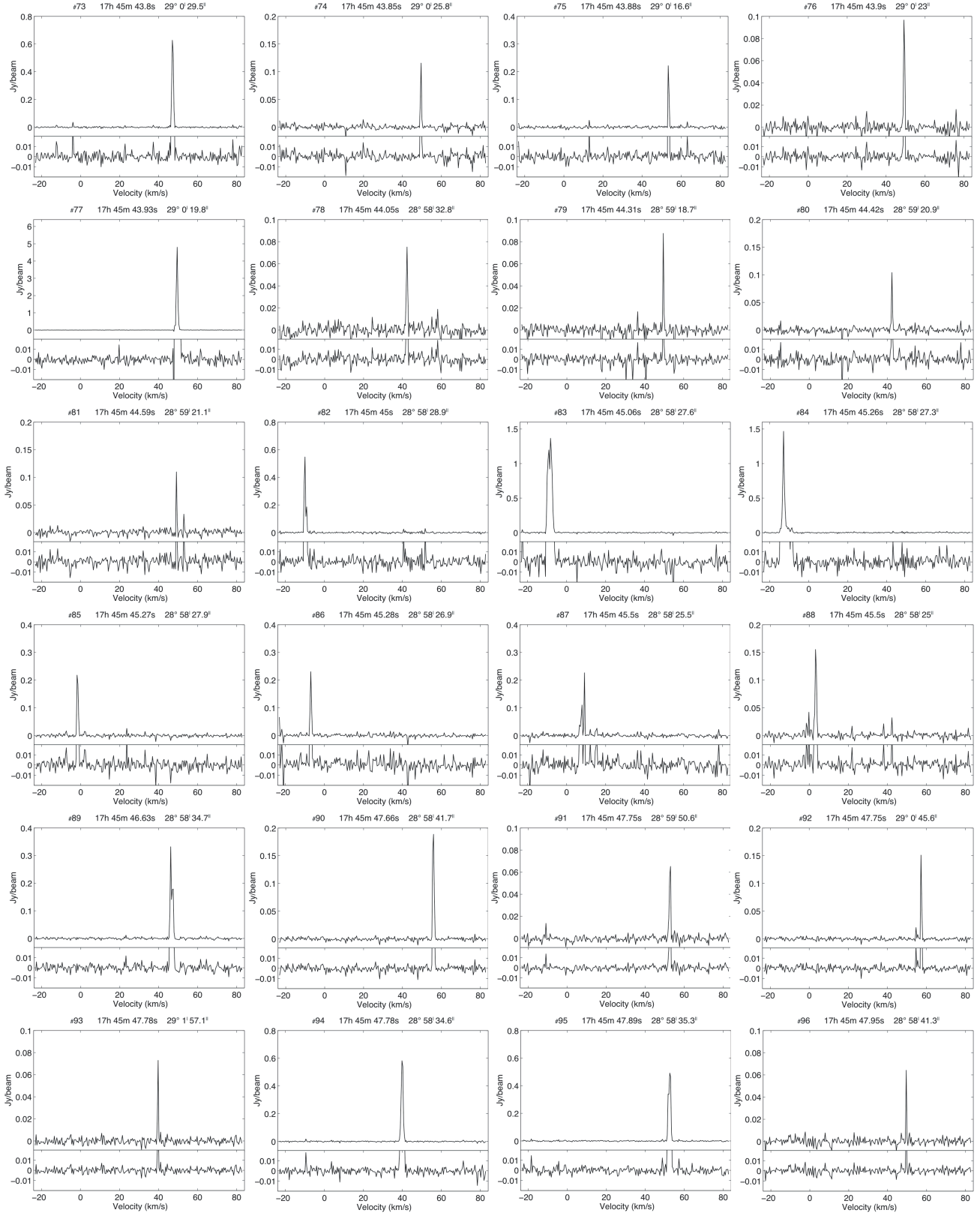
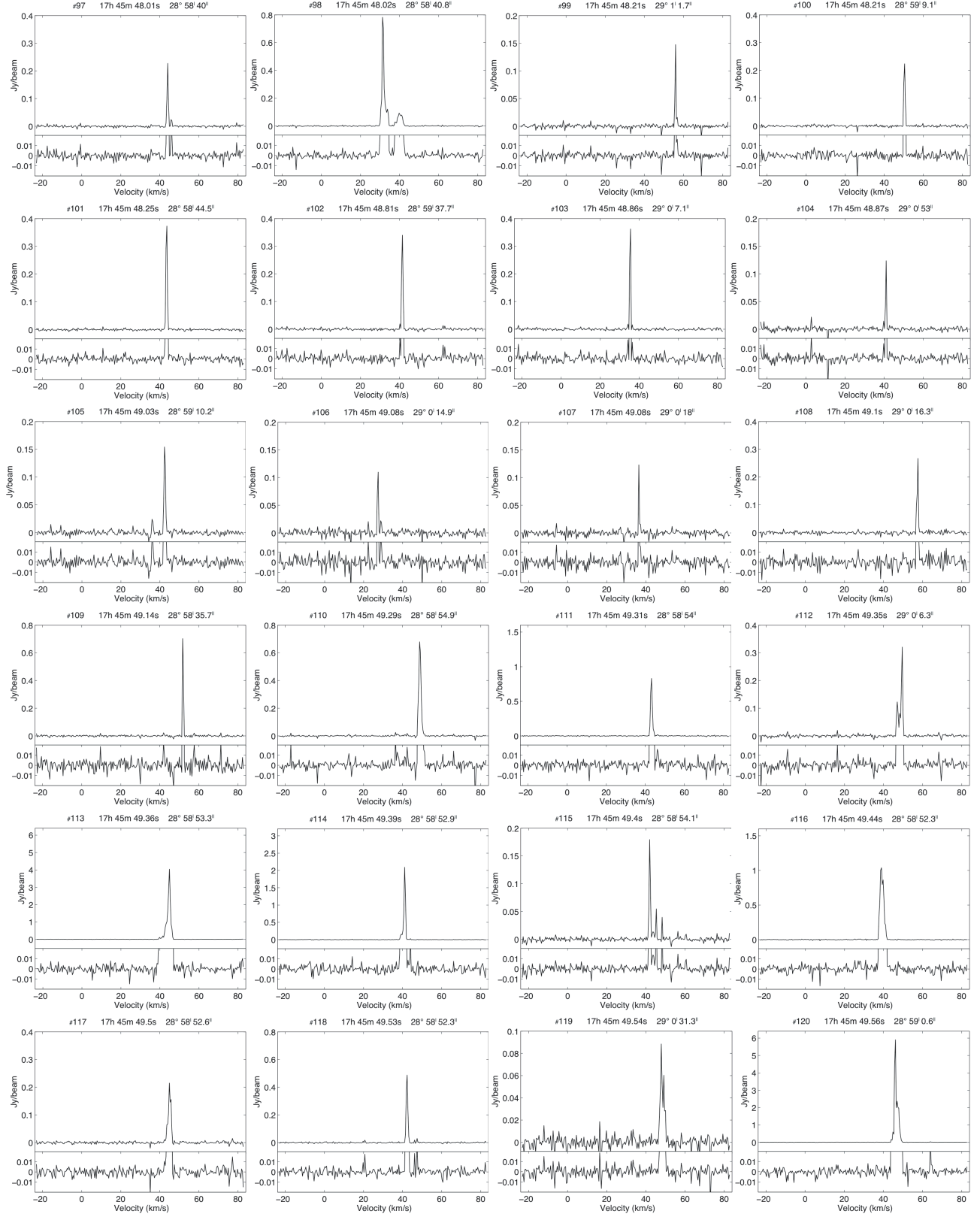


Figure 7. Example 44 GHz  $\text{CH}_3\text{OH}$  maser spectral profiles continued...

Figure 7. Example 44 GHz CH<sub>3</sub>OH maser spectral profiles continued...

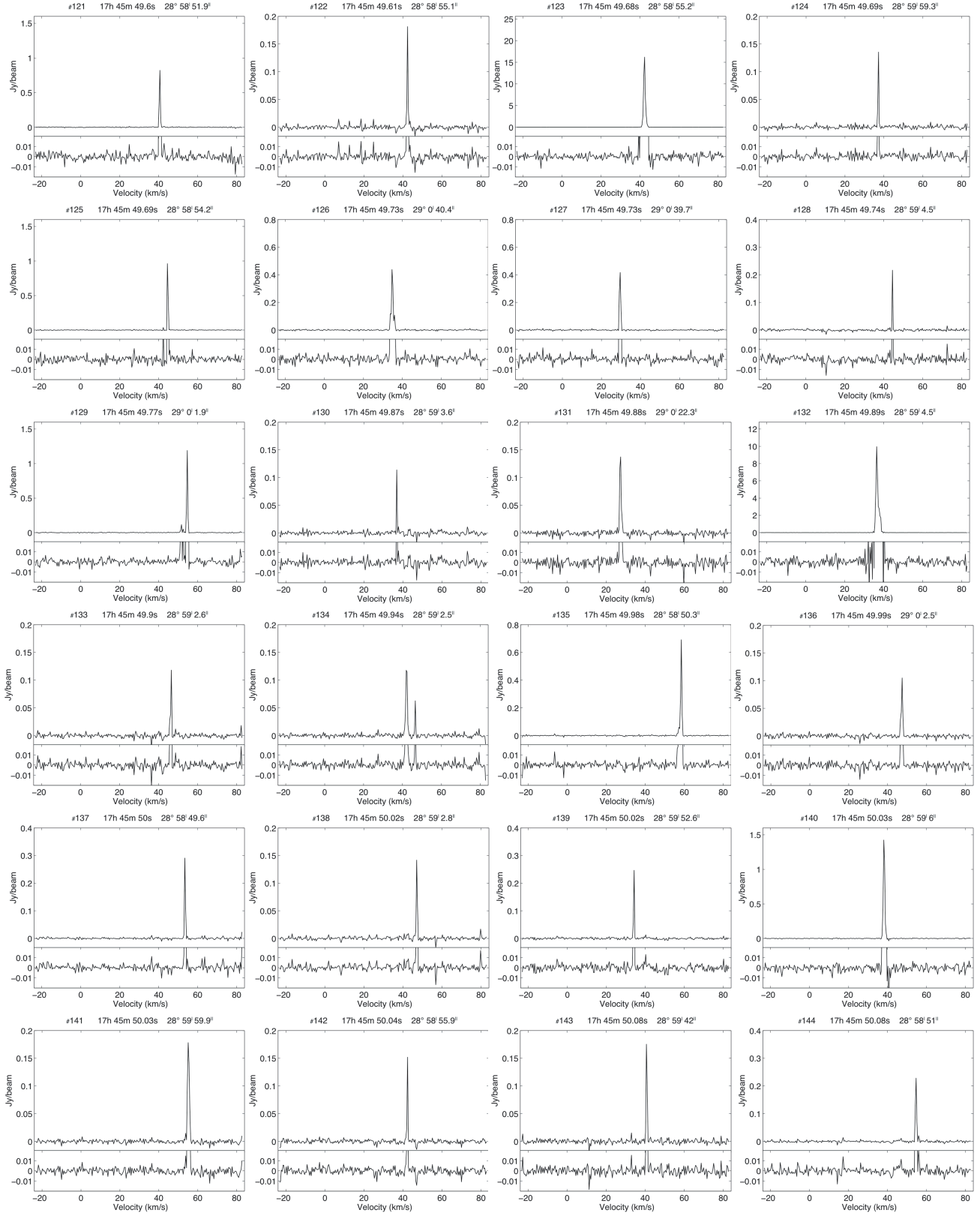
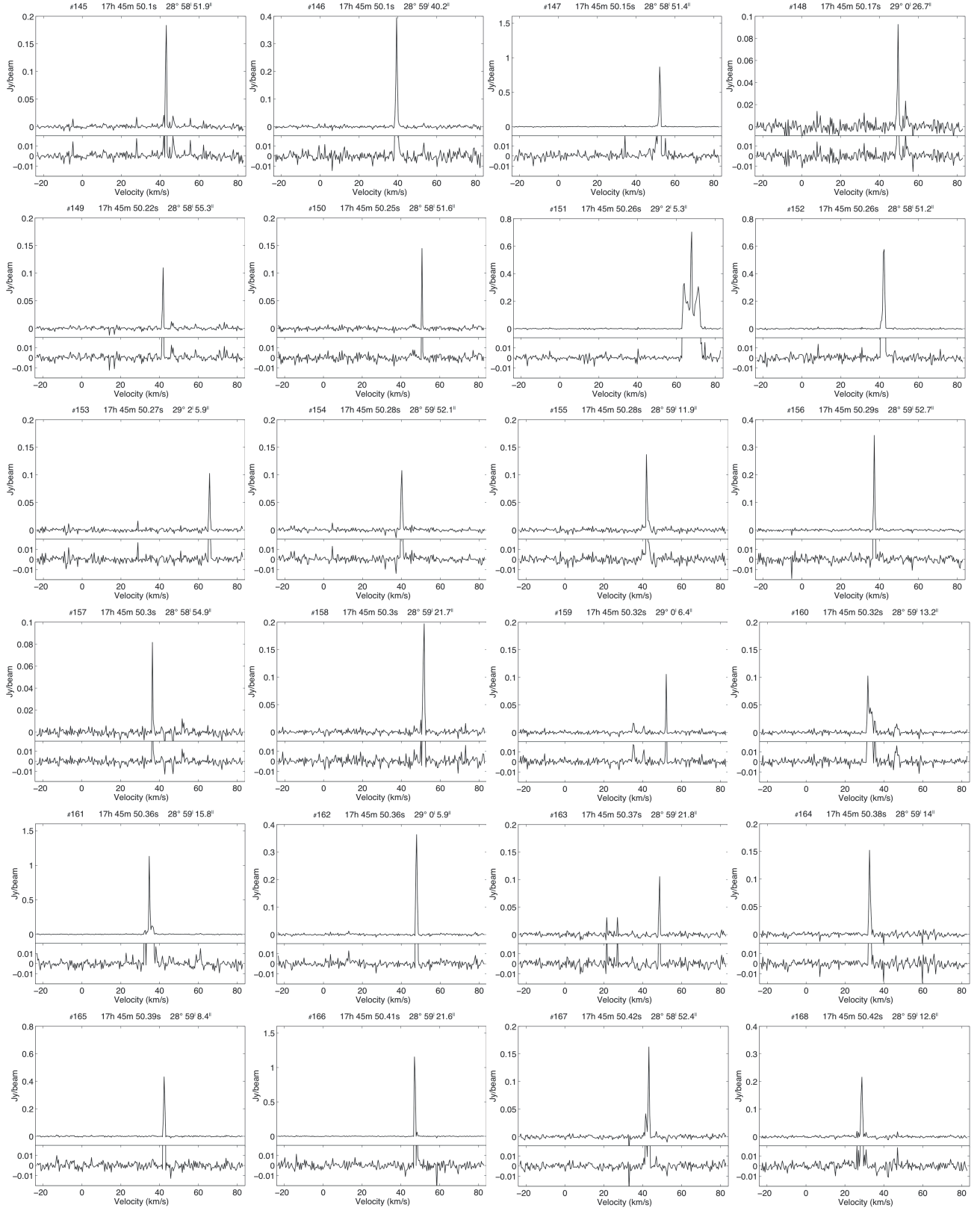


Figure 7. Example 44 GHz  $\text{CH}_3\text{OH}$  maser spectral profiles continued...



Figure 7. Example 44 GHz CH<sub>3</sub>OH maser spectral profiles continued...